Research Square

Preprints are preliminary reports that have not undergone peer review.
They should not be considered conclusive, used to inform clinical practice,
or referenced by the media as validated information.

Genetic architecture of incretin and glucagon regulation revealed by genome and exome-wide analysis in the Fenland cohort

Nicholas J Wareham

njw1004@cam.ac.uk

Institute of Metabolic Science (IMS) Epidemiology

Rofaida A Desoki

Institute of Metabolic Science (IMS) Epidemiology

Jack Murzynowski

University of Cambridge https://orcid.org/0009-0000-5341-2322

Isobel D Stewart

Institute of Metabolic Science (IMS) Epidemiology

Felix Day

University of Cambridge

Jian'an Luan

University of Cambridge

Nicola Kerrison

University of Cambridge

Katherine A Kentistou

Institute of Metabolic Science (IMS) Epidemiology

Mairi Antypa

Institute of Metabolic Science (IMS) Epidemiology

Thomas Hodkinson

Institute of Metabolic Science (IMS) Epidemiology

Vasileios Kaimakis

Institute of Metabolic Science (IMS) Epidemiology

Adam Davison

University of Cambridge,

Sofia Aleksashina

Institute of Metabolic Science (IMS) Metabolic Research Laboratories

Gareth Rogers

Institute of Metabolic Science (IMS) Metabolic Research Laboratories

Rula Bany Bakar

University of Cambridge https://orcid.org/0000-0002-5643-0195

Fiona M Gribble

Institute of Metabolic Science (IMS) Metabolic Research Laboratories

Frank Reimann

University of Cambridge

Claudia Langenberg

Queen Mary University of London https://orcid.org/0000-0002-5017-7344

John Perry

Medical Research Council Metabolic Diseases Unit, Institute of Metabolic Science-Metabolic Research Laboratories, Cambridge, UK

Matthew Coghlan

Eli Lilly and Company https://orcid.org/0000-0002-0894-1505

Pallav Bhatnagar

Lilly, Inc

Ken Ong

Medical Research Council Metabolic Diseases Unit, Institute of Metabolic Science-Metabolic Research Laboratories, Cambridge, UK

Article

Keywords:

Posted Date: November 9th, 2026

DOI: https://doi.org/10.21203/rs.3.rs-11352998/v1

License: This work is licensed under a Creative Commons Attribution 4.0 International License.
Read Full License

Additional Declarations:
Yes there is potential Competing Interest. Conflict of Interest Statement NJW and CL held a research grant with the University of Cambridge from Eli Lilly to support the GLP1, GIP and glucagon measurements in the Fenland study. RD's clinical PhD Fellowship was supported by a grant from Eli Lilly. MC and PB are employees of Eli Lilly.

Table 2 is available in the Supplementary Files section.

Genetic architecture of incretin and glucagon regulation revealed by genome and exome-wide analysis in the Fenland cohort

Rofaida Desoki[1,2], Jack R.A. Murzynowski[1], Isobel D Stewart[1], Felix R Day[1], Jian'an Luan[1], Nicola D. Kerrison[1], Katherine A. Kentistou[1], Mairi Antypa[1], Thomas Hodkinson[1], Vasileios Kaimakis[1], Sofia Aleksashina[3], Adam Davison[3], Gareth Rogers[3], Rula Bany Bakar[3], Claudia Langenberg[4,5,6], John R.B. Perry[1], Fiona M Gribble[3], Frank Reimann[3], Matthew Coghlan[7]*, Pallav Bhatnagar[7]*, Ken K Ong[1]*, Nicholas J Wareham[1]*

**Senior and corresponding authors*
Corresponding Authors' emails:
Matthew Coghlan: coghlan_matthew@lilly.com
Pallav Bhatnagar: bhatnagar_pallav@lilly.com
Ken K Ong: ken.ong@ims.cam.ac.uk
Nicholas J Wareham: njw1004@cam.ac.uk

Affiliations:

[1]Institute of Metabolic Science (IMS) Epidemiology, University of Cambridge, Box 285 Cambridge Biomedical Campus, Cambridge CB2 0QQ, UK.

[2]Genetics Department and Clinical Genomics Centre, Faculty of Medicine, Alexandria University, Alexandria, Egypt.

[3]Institute of Metabolic Science (IMS) Metabolic Research Laboratories, University of Cambridge, Cambridge Biomedical Campus, Cambridge, CB2 0QQ, UK.

[4]Precision Healthcare University Research Institute, Queen Mary University of London, London, UK.

[5]Computational Medicine, Berlin Institute of Health at Charité - Universitätsmedizin Berlin, Berlin, Germany.

[6]DZHK (German Centre for Cardiovascular Research), partner site Berlin, Berlin, Germany.

[7]Lilly Research Laboratories, Eli Lilly and Company, Indianapolis, IN 46225, USA.

Abstract

The receptors for glucagon and incretin hormones: glucose-dependent insulinotropic peptide (GIP) and glucagon-like peptide-1 (GLP-1), are key therapeutic targets for Type 2 diabetes (T2D) and obesity treatments. To better understand the metabolic hormones biology, we performed genome-wide association study (GWAS), and exome-based rare-variant analysis for immunoassay-measured GIP, GLP-1 and glucagon at fasting (T0) and 120-minutes post-oral glucose load (T120) in the Fenland Study.

We identified 16 GWAS associations including 5 at T0 including at *PDE3B* with glucagon$_{T0}$, and 10 at T120 including at *SLC38A4* with glucagon$_{T120}$, highlighting the value of hormone measures post-glucose load. We demonstrated high expression of *Slc38a4* in mouse α-cells, and SLC38A4 amino acid substrates triggered calcium influx and glucagon secretion. Secondary analysis of hormonal change (T120-T0) highlights *ANO1* with GIP$_{(T120-T0)}$. We also showed that cAMP-stimulated GIP secretion was abolished in *ANO1* knockout duodenal organoids.

Rare-variant analysis identified 6 associations, including *GCGR.* Links between *PDE3B* with glucagon and central adiposity emerged across both common and rare-variant analyses. These findings implicate biologically actionable pathways and provide a genetic foundation for mechanistic investigations and optimising metabolic disease therapeutics.

Introduction

Glucose-dependent insulinotropic peptide (GIP), glucagon-like peptide-1 (GLP-1), and glucagon are peptide hormones whose receptors are key therapeutic targets for a growing number of effective treatments for Type 2 diabetes (T2D) and obesity. GIP and GLP-1 are incretins, which stimulate insulin secretion after oral ingestion of glucose; GLP-1 also suppresses glucagon secretion and appetite; while glucagon counteracts hypoglycaemia[1]. These three hormones orchestrate complex responses extending beyond their classical roles in glucose homeostasis, with effects on appetite, cardiovascular health, energy storage and bone remodelling[2-5].

Given the modulation of these hormones with food intake, there is interest in studying their levels in response to an oral glucose load and understanding their biological regulation. Almgren *et al*.[6] reported 6 genome-wide association study (GWAS) signals for GIP and GLP-1: a signal at *SLC5A1* for both GIP and GLP-1 at 120 minutes post-glucose load, and a further 5 signals for GIP alone, but none for glucagon. Other studies have reported further associations with GIP and glucagon as measured by the proteomic platforms; SomaScan[7-9] and Olink[10,11]. However, knowledge of the genetic architecture of these hormones remains limited and inconsistent, constrained by small cohort sizes[6,8,12], reliance on common variant genotypes from GWAS arrays[6], and the use of proteomic platforms that lack specificity[7,9,13].

We aimed to assess the common (minor allele count; MAF>1%) and rare genetic architecture (MAF<1%) of incretins and glucagon, quantified using high specificity immunoassay, and to identify biologically actionable pathways relevant to metabolic disease therapeutics. We generated and analysed data from over 10,000 European ancestry participants from the Fenland Study, a UK based cohort with array and whole exome sequencing (WES) data[14]. We quantified circulating levels of GIP, GLP-1 and glucagon both while fasting (T0), and at 120 minutes post-glucose load (T120). We also sought to functionally validate the links of *SLC38A4* and *ANO1* to associated hormones, serving as a 'genetics-to-mechanism' blueprint by investigating their cellular dynamics. We demonstrate how the genetics of glucagon regulation can resolve the links between clinical hyperglucagonemia and its underlying molecular drivers.

Results

In the Fenland Study, median (IQR) age was 48.8 (42.7-54.6) years, BMI was 26.2 (23.6-29.4) kg/m^2 and 53.8% of participants were female (**Table 1**). None had known diabetes at baseline, but 214/12383 (1.7%) had undiagnosed diabetes on study biochemistry (see **methods**). We measured the levels of total GIP (pg/mL), total GLP-1 (pM) and glucagon (pM) in up to 10,874 participants using a tailored MSD U-PLEX immunoassay. Measurements were performed on plasma samples collected following an overnight fast (T0) and also 120-minutes after a 75-g oral glucose load (T120); we also calculated change between timepoints (T120-T0) for each hormone. Median (IQR) fasting and postprandial levels were 67.8 (49.2-94.2) and 378.1

(274.1-508.9) pg/mL for GIP; 27.7 (22-36) and 43.1 (32.4-59.6) pM for GLP-1; and 51.3 (37.3-71.3) and 37.8 (28.4-50.5) pM for glucagon. All values were inverse rank normal transformed for downstream analyses.

Phenotypic correlations

Weak to moderate phenotypic correlations were observed between T0 and T120 measures for each hormone (GIP, Pearson's r =0.35; GLP-1, r =0.18; glucagon, r=0.51; Supplementary Table 1.1). This supports the possibility of distinct genetic architectures between fasting and post-glucose states. There were moderate correlations between hormones measured at the same timepoint; GLP-1 and glucagon at both T0 (r=0.59) and T120 (r=0.50). GIP was more weakly correlated with GLP-1 (T0, r=0.28; T120, r=0.35; Supplementary Table 1.2). GIP, GLP-1 and glucagon all showed variable correlations with other metabolic traits (BMI, HbA1c, and insulin and glucose at T0 and T120). Insulin_{T0} was most strongly correlated with glucagon_{T0} (Spearman's ρ=0.43) and GLP-1_{T0} (ρ=0.33). BMI also correlated with both glucagon_{T0} (ρ=0.31) and GLP-1_{T0} (ρ=0.25, **Supplementary Table 1.3**).

Given that both glucagon and GLP-1 are products of the same proglucagon precursor, we examined the correlations of their MSD-measured T0 levels with Olink-measured fasting proglucagon in 483 Fenland Study participants. Olink proglucagon was strongly correlated with GLP-1_{T0} (Pearson's r=0.71), and weakly correlated with glucagon_{T0} (r=0.36; **Supplementary Table 1.4**).

Genetics of peptide hormones

GWAS on common variants (minor allele count; MAF >1%) for all hormones were performed in up to 9,988 European ancestry individuals at both time points (**Supplementary Table 2**). The narrow-sense heritability, estimated using GCTA-GREML, at T0 and T120 was for GIP: 12.6% and 24.3%; for GLP-1: 4.6% and 15.3%; and for glucagon: 18.2% and 22.3% respectively (**Supplementary Table 2**). Independent association signals ($P<5.0\times10^{-8}$) were identified by distance-based (+/− 250kb) clumping. We then linked these signals to likely causal genes using the "GWAS-to-gene" (G2G) bioinformatic pipeline[15], including conditional analysis by GCTA-COJO, and amalgamating several sources of genomic and functional evidence.

In total, we identified 16 common variant-hormone associations (**Table 2**) (**Figure 1-4**). For GIP, 5 signals were identified. At *GIPR,* there were associations at both timepoints; 3 further signals associated with GIP_{T120}, one of which - *FUT3* - was novel. Two signals were found for GLP-1 including a novel GLP-1_{T0} association at *ABHD15*. For glucagon, 8 signals were identified (5 at T120 and 3 at T0), none of which have been reported previously. Secondary analysis of the change in hormone levels highlighted an additional novel gene; *ANO1*, associated with $\text{GIP}_{T120\text{-}T0}$.

Figure 1. Overview of common and rare variant association analyses for GIP, GLP-1 and glucagon measured at fasting (T0) and 120 minutes post-oral glucose (T120).

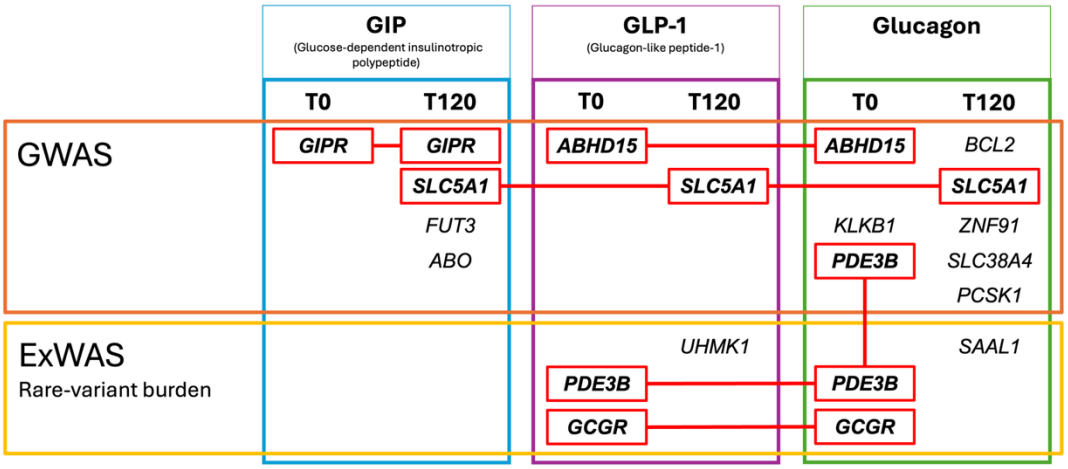
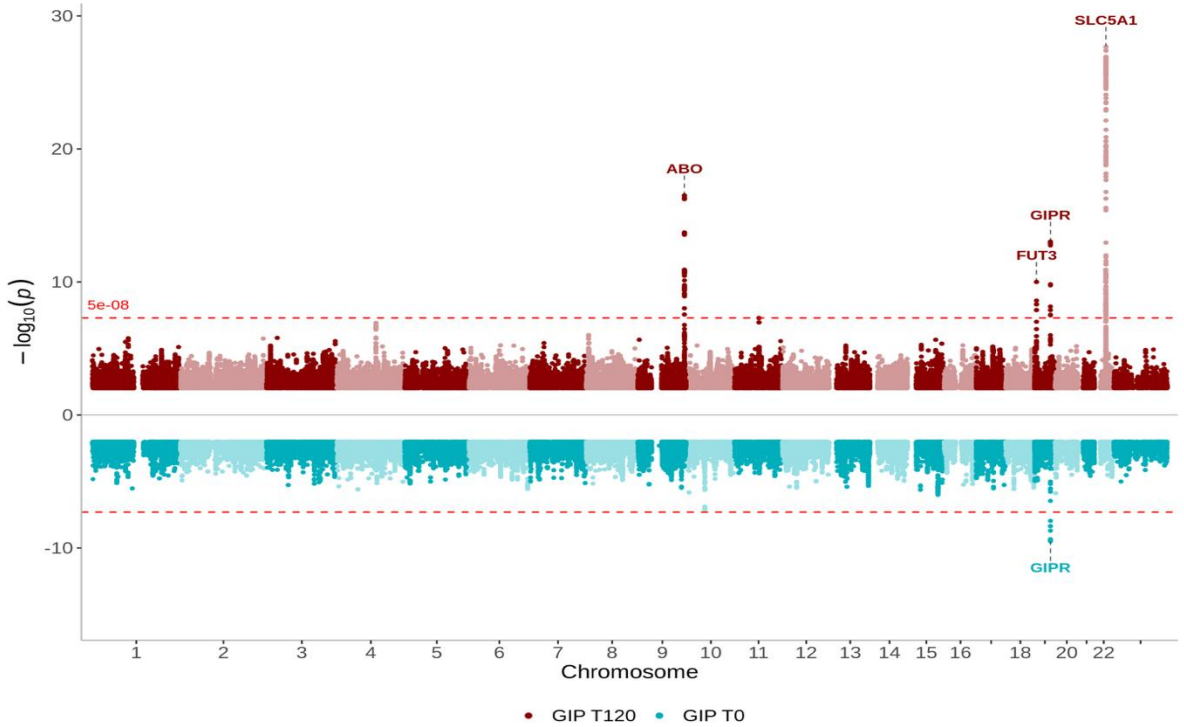
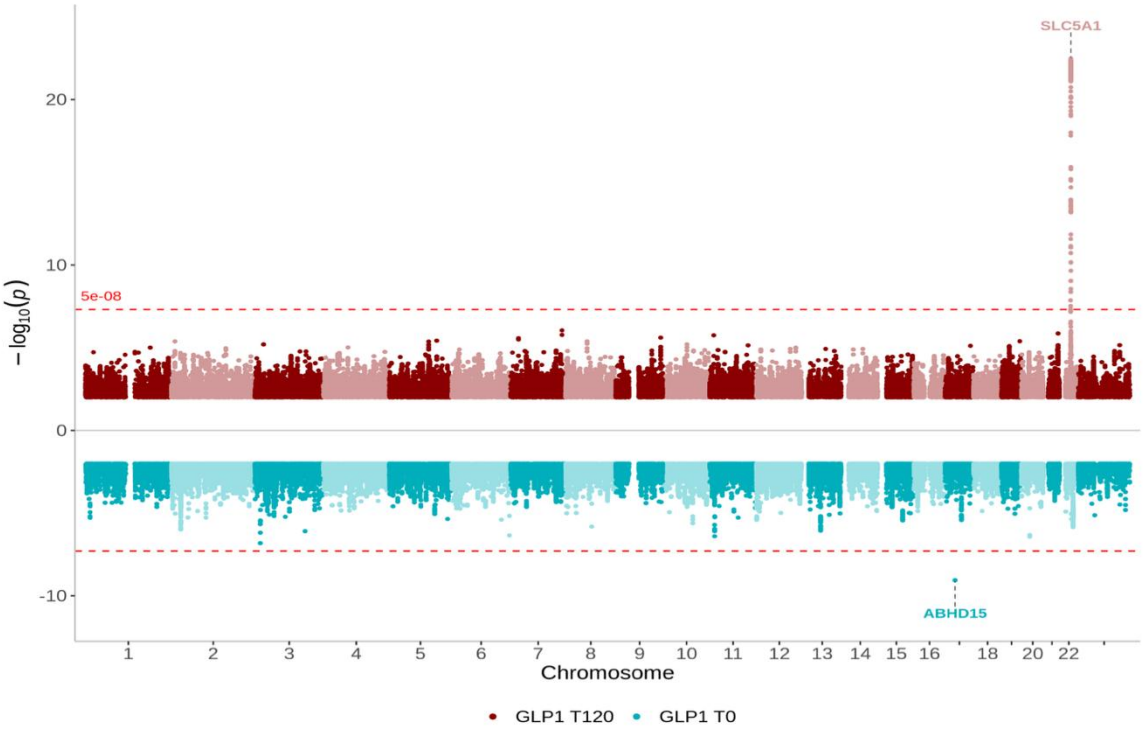


Figure 2. Miami plot for GWAS results of GIP measured at fasting (T0) and 120 minutes post-oral glucose (T120).



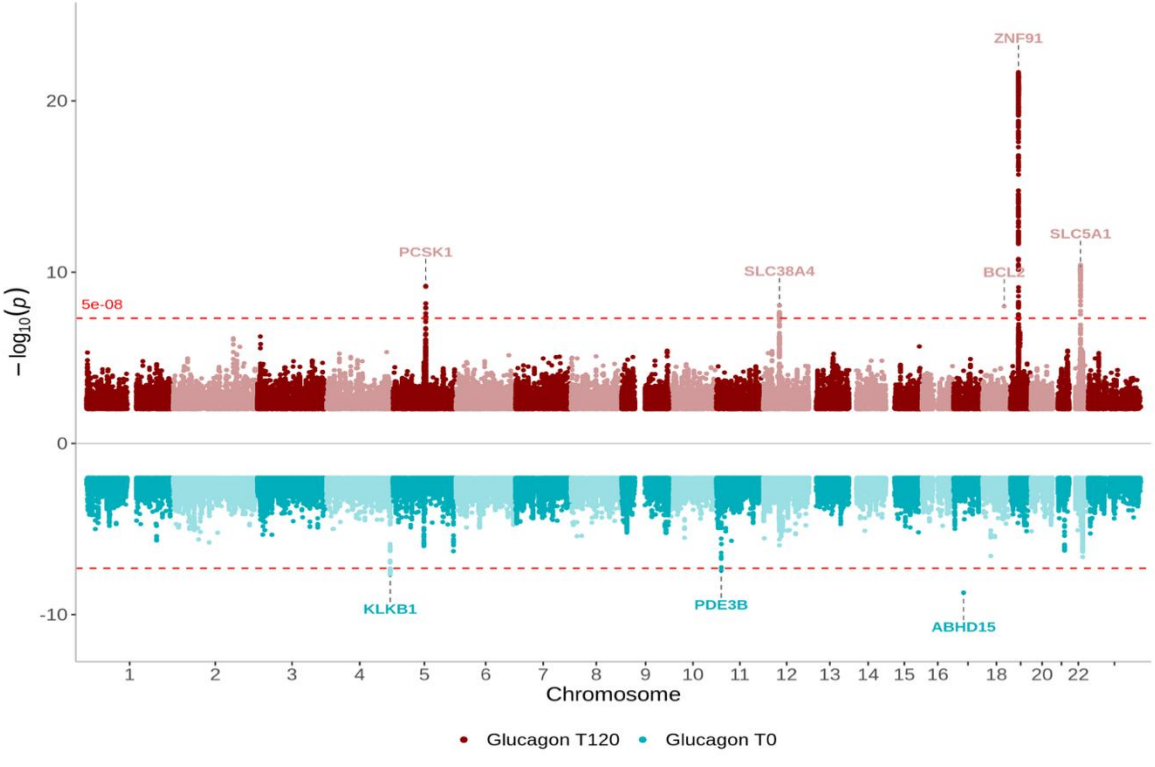
Miami plot showing GIP GWAS results with gene annotation as identified by the GWAS-to-gene (G2G) pipeline. Red dotted lines indicate genome-wide significance threshold at $p = 5\times10^{-08}$. The top panel displays the GWAS of GIP at T120. The bottom panel displays results from the GIP at T0 GWAS.

Figure 3. Miami plot for GWAS results of GLP-1 measured at fasting (T0) and 120 minutes post-oral glucose (T120).



Miami plot showing GLP-1 GWAS results with gene annotation as identified by the G2G pipeline. Red dotted lines indicate genome-wide significance threshold at $p = 5\times10^{-08}$. The top panel displays the GWAS of GLP-1 at T120. The bottom panel displays results from the GLP-1 at T0 GWAS.

Figure 4. Miami plot for glucagon GWAS results measured at fasting (T0) and 120 minutes post-oral glucose (T120).



Miami plot showing Glucagon GWAS results with gene annotation as identified by the G2G pipeline. Red dotted lines indicate genome-wide significance threshold at $p = 5\times10^{-08}$. The top panel displays the GWAS of glucagon at T120. The bottom panel displays results from the glucagon at T0 GWAS.

Exome-wide gene-based rare-variant analyses (ExWAS) in up to 9,987 participants of European ancestry identified associations with 4 genes: *GCGR*, *PDE3B, SAAL1,* and *UHMK1* (**Table 3**). In *PDE3B*, also highlighted in our GWAS analysis for glucagon$_{T0}$, rare deleterious variants were collectively associated with both lower GLP-1$_{T0}$ and lower glucagon$_{T0}$. Furthermore, a stop-gained variant in *PDE3B* (rs150090666) was associated with both lower GLP-1$_{T0}$ and lower glucagon$_{T0}$. At the glucagon receptor gene, *GCGR*, deleterious variants burden was associated with higher glucagon$_{T0}$ and higher GLP-1$_{T0}$. Deleterious variants burden in *SAAL1* was associated with lower glucagon$_{T120}$, and that in *UHMK1* was associated with higher GLP-1$_{T120}$.

Assessing the 13 genes highlighted by GWAS across the rare-variant burden results, in addition to *PDE3B,* deleterious variants burden in *SLC5A1* was associated with lower GIP $_{T120}$ at sub-exome-wide significance (p=1.7×10^{-5}, **Supplementary Table 8**).

Common variant signals at SLC5A1 and ABHD15 show associations across hormones

Reflecting the possible shared biology of these hormones, 2 loci were associated with multiple hormones: *SLC5A1* (GIP$_{T120}$, GLP-1$_{T120}$, and glucagon$_{T120}$) and *ABHD15* (GLP-1$_{T0}$ and glucagon$_{T0}$).

Associations at *SLC5A1* were previously reported with GIP and GLP-1[6]. Here we replicated those (rs115866486; MAF 0.075; GIP$_{T0}$ p=2.1×10^{-28}; GLP-1$_{T120}$: p=3.3×10^{-23}) and identified a novel association with glucagon$_{T120}$ (rs117983733, r^2= 0.97, p=3.8×10^{-11}). *SLC5A1* encodes the sodium-dependent glucose transporter (SGLT1), which mediates gut absorption of glucose and galactose[16,17]. It acts as a glucose sensor that triggers the secretion of GIP and GLP-1[18] and has been implicated in the regulation of glucagon secretion[19-21]. Surprisingly, associations with *SLC5A1* were directionally concordant across all 3 hormones, but with lowest effect size on glucagon$_{T120}$. We propose that the glucagon effect is mediated through GIP given that the rare deleterious variants association with *SLC5A1* was only apparent for GIP $_{T120}$ (p=1.7×10^{-5}, **Supplementary Table 5**). This is supported by the known glucagon-stimulant effect of GIP at lower glucose levels[22]. The sentinel GIP$_{T120}$-increasing T allele confers higher expression of *SLC5A1*[23]. SGLT1 is one of the targets, along with SGLT2, of Sotagliflozin, a medication approved to reduced risk of cardiovascular complications in patients with Type 2 diabetes and other cardiometabolic risk factors[24].

The associations at *ABHD15* (rs542939, p.Thr334Ala, GLP-1$_{T0}$: p=8.7×10^{-10} and glucagon$_{T0}$: p=1.9×10^{-9}) were also directionally concordant. *ABHD15* encodes Alpha/Beta Hydrolase Domain-Containing Protein 15, known to influence insulin signalling in adipocytes to suppress lipolysis[25], possibly by its interaction with, and stabilization of, phosphodiesterase 3B (Pde3b)[26-28]. The GLP-1$_{T0}$- and glucagon$_{T0}$-increasing allele also confers higher *ABHD15* expression in blood[29], and was previously modestly associated with higher levels of Olink proglucagon (p=1.3×10^{-4})[23]. Rare non-synonymous variants in both *ABHD15* and *PDE3B* were

previously associated with higher WHR_{adjBMI}[30], suggesting their possible roles in mediating glucagon actions on central adiposity.

Rare variant associations support PDE3B and highlight the glucagon receptor

Unlike *ABHD15*, the common variant at *PDE3B* was significant only with $glucagon_{T0}$ (rs61883634, $p=3.7\times10^{-8}$) but also showed sub-threshold association with GLP-1_{T0} ($p=3.9\times10^{-7}$). Independent evidence from rare-variant analysis robustly linked deleterious variants burden in *PDE3B* to both lower $glucagon_{T0}$ ($p=9.9\times10^{-11}$, $n=102$ carriers) and lower GLP-1_{T0} ($p=1.2\times10^{-9}$, $n=30$). *PDE3B* encodes an enzyme that hydrolyses cAMP and cGMP with an established role in glucose-induced insulin secretion[31] and the insulin-mediated inhibition of lipid catabolism[27]. In our data, rs61883634 appeared independent of the extensively studied and exome-based significant rare stop-gained variant in *PDE3B* (rs150090666, p.Arg783Ter; $r^2=0.02$, $D'=0.87$; MAF 0.12%, $glucagon_{T0}$ $p=1.5\times10^{-6}$), as its association persisted after adjusting for rs150090666 – $p=2.3\times10^{-5}$ after adjustment. Previous exome studies also linked rs150090666 to lower total fat mass[32], weight[10] and high-density lipoprotein cholesterol[33,34], but higher triglyceride[35,36], WHR_{adjBMI}[37], and cardiovascular disease risk[30,38]. Our evidence supports the role of PDE3B in regulating glucagon secretion, and possibly thence to other metabolic traits. PDE3B is targeted by the non-selective phosphodiesterase inhibitor; Pentoxifylline, approved to treat peripheral vascular disease.

The glucagon receptor (encoded by *GCGR*), preferentially couples to *Gs* proteins, stimulating adenylyl cyclase to produce cAMP and triggering downstream signalling cascades[39], while PDE3B hydrolyses cAMP. During high systemic glucose demand, glucagon activates this pathway to drive hepatic glycogenolysis and gluconeogenesis[40]. At *GCGR*, deleterious variants burden was associated with higher $glucagon_{T0}$ and GLP-1_{T0} ($p=2.7\times10^{-15}$, $n=49$; and $p=1.2\times10^{-7}$, $n=48$, respectively). This association suggests a milder form of the rare disorder Mahvash disease which is caused by homozygous inactivating *GCGR* mutations and characterised by hyperglucagonemia.

A third rare deleterious variant association was identified with *UHMK1* and higher GLP-1_{T120} levels ($p=2.7\times10^{-6}$; $n=106$) which, unlike *GCGR* and *PDE3B*, was not associated with glucagon. *UHMK1* (U2AF Homology Motif Kinase 1) encodes a serine/threonine-protein kinase and is highly expressed in neurons and endocrine tissues[41]. UHMK1 is implicated in the regulation of vesicle secretion, and links secretory vesicle dynamics to downstream gene expression[42], suggesting a role in GLP-1 secretion.

GWAS for GIP replicates known signals and identifies FUT3

We were able to replicate previously reported GWAS associations at *GIPR*[6] with both GIP_{T0} and GIP_{T120} (rs10423928, $p=3.3\times10^{-10}$ and $p=9.4\times10^{-14}$ respectively). Our study lead variant is in high LD ($r^2=0.99$) with the previously reported GIP_{T0} and GIP_{T120} associated missense

variant (rs1800437 [E354Q])[6]. We also replicated the association at *ABO* (rs8176685, GIP_{T120}: $p=3.1\times10^{-17}$). Here, the GIP_{T120}-increasing allele also confers higher *ABO* expression in blood (GTEx V10) and is in high LD with the previously reported signal rs635634 ($r^2= 0.98$)[6].

A novel signal for GIP_{T120} implicated *FUT3* (rs2608894, $p=1.0\times10^{-10}$) which, like *ABO,* is involved in the blood group system. *FUT3* encodes fucosyltransferase 3, which catalyses the final step in the biosynthesis of Lewis histo-blood group antigens[43-45]. Our GIP_{T120}-increasing allele colocalises with the enzyme fucosyltransferase 3-increasing allele of rs708686– a cis-protein quantitative trait locus[13,46]. Individuals with Lewis-negative genotypes (with expected lack of fucosyltransferase 3 activity) have reports of lower fasting glucose, suggesting a role in glucose homeostasis[47]. We found no clear evidence linking rs2608894 to T2D risk, but the GIP_{T120}-increasing allele has been reported to be associated with lower fasting insulin ($p=3.6\times10^{-3}$, **Supplementary Table 5**).

Genetic architecture of glucagon

Glucagon showed the greatest number of GWAS signals, including 5 signals that did not overlap with GIP and GLP-1.

The lead variant rs4253281 for $glucagon_{T0}$ ($p=2.1\times10^{-8}$) implicated *KLKB1* which encodes prekallikrein, and has been implicated in regulating blood pressure, inflammation and coagulation pathways[48]. Kallikrein is the target of a number of existing mediations that are used to treat angioedema, including the monoclonal anti-body treatment Lanadelumab.

SLC38A4 implicated by lead variant rs7976518 for $glucagon_{T120}$ ($p=8.7\times10^{-9}$), encodes a sodium-coupled amino acid transporter (SNAT4/ATA3) which facilitates transmembrane transport of cationic and neutral amino acids, preferentially smaller ones with unbranched side chains[49,50]. It is highly expressed in the liver and skeletal muscle (GTEx V10). The $glucagon_{T120}$-increasing (major T) allele confers higher *SLC38A4* expression (GTEx V10) and corresponds to the G allele of rs11183644 ($r^2=0.99$) which confers increased splicing of *SLC38A4* in skeletal muscle[51]. The $glucagon_{T120}$-increasing allele is also strongly associated with lower alanine ($p=2.8\times10^{-21}$), glutamine, tyrosine and ornithine levels[52]. We further characterised *SLC38A4* expression and function below.

PCSK1 encodes prohormone convertase (PC)1/3, which is known to cleave various prohormones, including proglucagon into GLP-1[53-55]. Loss-of-function mutations in *PCSK1* cause hyperphagic obesity and malabsorptive diarrhoea[56,57]. Patients with monogenic PC1/3 deficiency have reported normal fasting glucagon levels but impaired GLP-1 secretion post-OGTT[58]. Surprisingly, we find a common variant association between *PCSK1* and $glucagon_{T120}$ (rs3762985, $p=6.6\times10^{-10}$), but not GLP-1 (or GIP) at either time point ($p>0.05$), suggesting that *PCSK1* is may also be involved in glucagon regulation in response to glucose.

The association between rs12974550 and $glucagon_{T120}$ ($p=2.1\times10^{-22}$) implicated *ZNF91* which encodes Zinc Finger Protein 91. The $glucagon_{T120}$-increasing allele also confers higher *ZNF91* splicing (GTEx V10), and higher Olink proglucagon levels ($p=7.5\times10^{-7}$)[23].

The lead variant rs72943036 for glucagon$_{T120}$ (p=1.0×10^{-8}) implicated the evolutionarily conserved gene *BCL2*, which encodes anti-apoptotic B-Cell Leukemia 2, a critical inhibitor of the intrinsic apoptotic pathway. The glucagon$_{T120}$-increasing allele is also nominally associated with lower *BCL2* expression (GTEx V10: p=1.2×10^{-5}). Interestingly, *BCL2* overexpression is a hallmark of various malignancies, leading to the development of targeted BCL-2 inhibitors like Venetoclax that restore apoptosis in anticancer therapy[59].

Finally, rare deleterious variants burden in *SAAL1* was associated with lower glucagon$_{T120}$ (p=2.6×10^{-6}; n = 21). SAAL1 (Serum Amyloid A-Like 1) is synthesized by hepatocytes as an acute-phase protein[60], is upregulated in synovial fibroblasts from rheumatoid joints[61] and was recently identified as an oncogene in hepatocellular carcinoma[62].

GWAS for hormonal changes (T120-T0) highlights ANO1

As a secondary analysis, we performed GWAS for changes in levels of each hormone between timepoints (T120 minus T0). We identified 5 signals for GIP$_{T120\text{-}T0}$, 1 for GLP-1$_{T120\text{-}T0}$ and 2 for glucagon$_{T120\text{-}T0}$ (**Supplementary Table 3**). Seven of these were the same signals for the corresponding GWAS of T120 levels (**Supplementary Table 4**). The one novel signal, an intronic variant in *ANO1,* was associated with GIP$_{T120\text{-}T0}$ (rs902869, p=2.4×10^{-9}) and was borderline significant for GIP$_{T120}$ (p=5.1×10^{-8}). Here, the GIP$_{T120}$-increasing allele corresponds to the *ANO1* transverse colon expression-increasing allele of rs61885141 (r^2 = 0.39) (GTEx V10). *ANO1* encodes Anoctamin 1, a calcium-activated chloride channel responsible for trans-epithelial anion transport with high expression in secretory epithelial tissues including ileum, large intestine, exocrine pancreas and hepatocytes[63-65]. Notably, the GIP$_{T120}$-increasing allele at rs902869 is also reported to be associated with higher anion gap levels and cholelithiasis risk (p=4.9×10^{-3}, and p=4.7×10^{-14} respectively)[52].

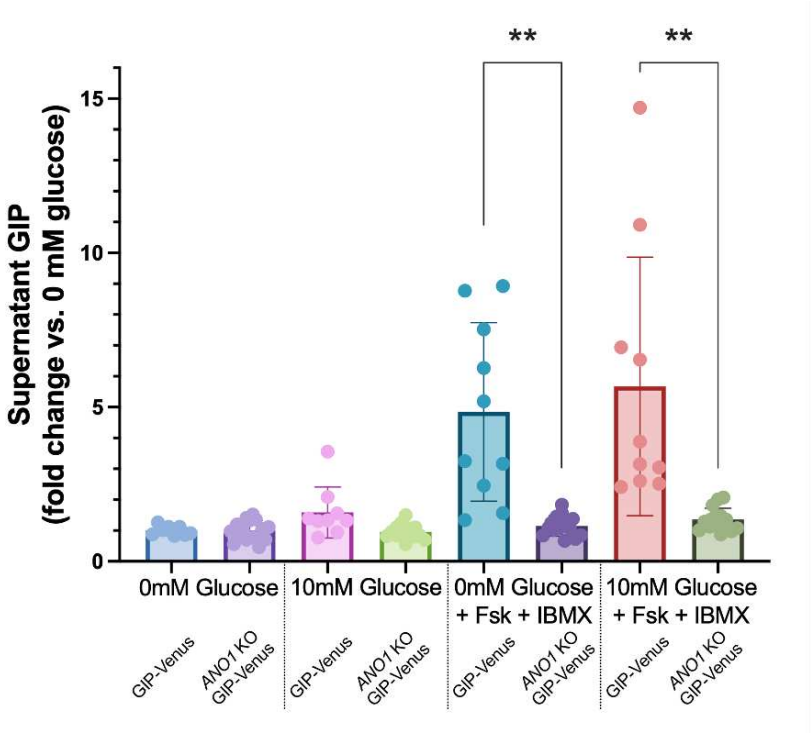
Functional studies have identified that ANO1-mediated cellular responses are initiated by the stimulation of G-protein-coupled receptors[66]. By facilitating chloride efflux, ANO1 promotes membrane depolarisation and amplifies calcium signalling, thereby regulating the magnitude of insulin secretion in response to glucose in beta cells[67]. Our data suggest a similar role of ANO1 in modulating GIP secretion. We therefore measured GIP secretion in wild-type (WT) and *ANO1* knock-out human duodenum-derived organoids to assess if ANO1 is implicated in stimulating GIP secretion from K-cells.

Functional analysis of ANO1 using GIP secretion assays

To determine whether the calcium-activated chloride channel ANO1 is implicated in the molecular mechanisms of GIP secretion from K-cells, we generated an *ANO1* knock-out line in human duodenal GIP-expressing organoids. GIP secretion assays were then performed to determine if absence of ANO1 affects hormone secretion. As glucose and elevated cAMP

(downstream of Gαs-coupled receptors[68]) are a known stimuli for GIP secretion from K-cells, supernatant GIP levels were measured using MSD under low (0mM) and high (10mM) glucose conditions[68]. ANO1 deletion did not significantly alter GIP secretion in either low or elevated glucose conditions. However in organoids treated with forskolin (10µM), an adenylate cyclase activator, and IBMX (100µM), a phosphodiesterase inhibitor, we observed that the increase in GIP secretion in wild type organoids, was largely abolished in the *ANO1* knock-out line (**Figure 5**). These data suggest that the ANO1 chloride channel is important for cAMP-mediated GIP secretion from human K-cells, supporting the *ANO1* human genetic association with GIP change.

Figure 1. Functional analysis of ANO1 using GIP secretion assays



GIP release from WT and ANO1 knock-out human duodenal organoids in response to stimulation with 0mM or 10mM glucose with or without application of Forskolin (10 µM) and IBMX (100µM). Data presented as mean ± SD of the fold change normalised to the average of the 0mM glucose basal treatments. n=8-15 replicates were obtained from 3 to 4 independent experiments. D'Agostino-Pearson test was used to assess the normality of the distribution, and unpaired t-test with Welch's correction was applied to test for

Associations of common variants signals with other metabolic traits

Across the signals we identified, there were notable patterns in their associations with other metabolic traits. Three of the 4 signals for GIP_{T120} are strongly associated with T2D, and in all cases the GIP_{T120}-increasing allele is associated with lower T2D risk. GIP_{T120} was the only hormone with signals that also associate with T2D (**Supplementary Table 5**), highlighting its potential role in insulin resistance. In addition to links to T2D at *SLC5A1*, both lead variants of incretin and glucagon hormones (rs115866486 and rs117983733 respectively) were linked to lower circulating branch chain amino acids (**Supplementary Table 5**). The association with amino acids other than loci (*PDE3B* and *SLC5A1)* which were significant after multiple testing, was also seen at two others at nominally significant thresholds (*ABO* and *SLC38A4*). As discussed later, functional analysis suggests shared regulation of the pathways that respond to glucose as those to amino acids.

Only two of the signals passed a multiple test correction ($p<4.3\times10^{-4}$) for an association with BMI. The signal at *GIPR* was genome-wide significant as reported previously[69], with GIP-increasing allele associating with higher BMI. We also show that the $glucagon_{T120}$ signal at *BCL2* appears to be linked to adiposity, but not to any blood sugar phenotypes, with $glucagon_{T120}$ -increasing allele associating with lower BMI.

At rs61883634-*PDE3B*, the $glucagon_{T0}$-increasing allele is associated with increased splicing of *PDE3B* in adipose tissue[51], higher branched-chain amino acids (BCAA) and confers higher WHR_{adjBMI} (**Supplementary Table 5**). While little is known about its role in glucagon secretion, *PDE3B* was recently linked to BCAA and lipid metabolism[31], which are established regulators of glucagon secretion[70-72]. This link to central adiposity was also seen with *PDE3B* rare deleterious variants associations with lower GLP-1, glucagon, WHR_{adjBMI} and alanine transaminase (ALT) levels after multiple test correction ($p<2.5\times10^{-3}$, **Supplementary Table 6**).

The $GLP\text{-}1_{T0}$- and $glucagon_{T0}$-increasing allele at *ABHD15* is also associated with lower HDL cholesterol and higher triglyceride[52]. Previous rare-variants burden associations of both *ABHD15* and *PDE3B* with higher WHR_{adjBMI}[30], reflect that both *PDE3B* and *ABHD15* are related to central adiposity.

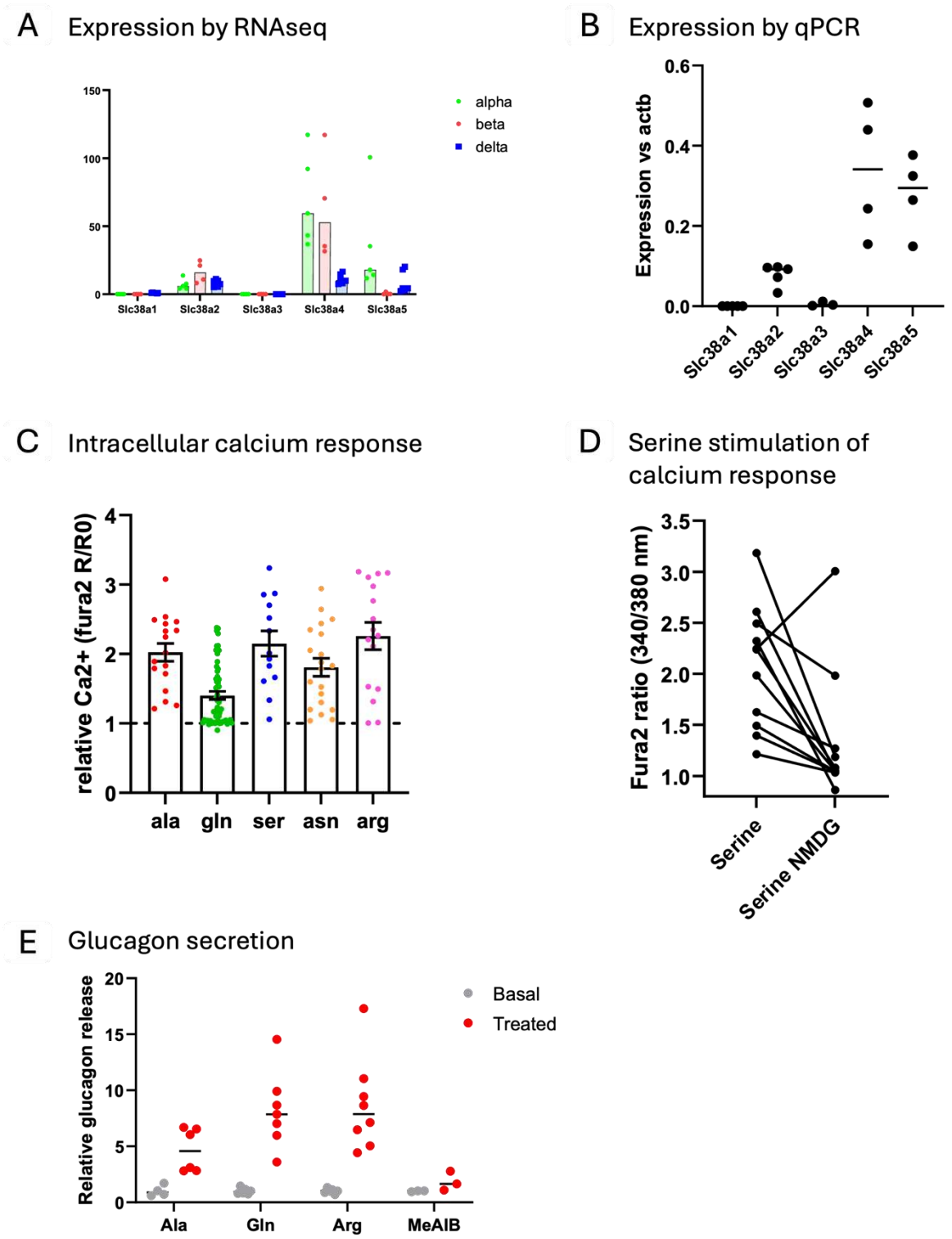
Replication of results from previous studies.

The only previous GWAS of individually-measured incretins and glucagon identified 8 signals[6]. We replicated 5 of them, namely at *GIPR* (for GIP_{T0} and GIP_{T120}), *ABO* and *SLC5A1* (GIP_{T120}), and *SLC5A1* ($GLP\text{-}1_{T120}$). These were among the strongest signals in our data for their respective hormones. However, we found no evidence for the remaining 3 signals, despite having high imputation quality (all INFO ≥0.99) and comparable allele frequencies in our data: *GLP2R* for GIP_{T0} (rs17681684, p=0.071); and *HOXD1* (rs150112597, p=0.03) and *F13A1* (rs927332, p=0.27) for GIP_{T120}.

Functional characterisation of SLC38A4 in alpha cells

In order to explore the *SLC38A4* signal identified in Glucagon$_{T120}$ GWAS, we used a mouse model to mechanistically characterise gene expression and cellular function. We demonstrated high expression of *Slc38a4* in mouse glucagon-producing pancreatic alpha cells through both RNA sequencing data and qPCR analyses (**Figure 6 a-b**). Indeed, *Slc38a4* was the most highly expressed of the well-characterised amino acid transporter group, *Slc38a1-5*, in murine pancreatic alpha-cells, reflecting similar results in human pancreas (https://sandberglab.se/tool/pancreas/). In isolated murine alpha cells, a range of amino acid substrates of SLC38A4 (alanine, serine, asparagine, glutamine and arginine) triggered rapid and robust elevations in intracellular calcium which were dependent on extracellular sodium, consistent with the involvement of a sodium-coupled electrogenic uptake pathway (**Figure 6 c-d**). Reassuringly, Slc38a4 substrate amino acids also triggered glucagon release from intact islets (**Figure 6 e**).

Figure 6. Functional characterisation of SLC38A4 expression, amino acid-induced calcium signalling, and glucagon secretion in pancreatic alpha cells.



(a) mRNA expression levels in isolated mouse glucagon-producing pancreatic alpha cells, of amino acid transporter group *Slc38a1-5,* determined by RNA sequencing. (b) Validation of amino acid transporter group *Slc38a1-5* expression in isolated mouse alpha cells measured by quantitative PCR (qPCR). (c) Intracellular calcium responses to 20mM of selected amino acids: alanine (ala), glutamine (gln), serine (ser), asparagine (asn), and arginine (arg) recorded in isolated murine alpha cells loaded with the ratiometric calcium indicator dye fura2-AM, with buffer containing 3mM glucose. Each data point represents the peak response of an individual alpha cell (n=1-7 alpha cells per dish, from 4-19 dishes). (d) Paired fura2 fluorescence ratios (340/380 nm) of individual alpha cells stimulated with Serine in standard sodium-containing buffer versus sodium-free buffer where sodium was replaced with *N*-methyl-*D*-glucamine (Serine NMDG). Lines connect responses from the same single cell. (e) Glucagon secretion profiles from isolated whole intact pancreatic islets in response to the indicated amino acids administered at a concentration of 10mM as following: alanine (ala), glutamine (gln), arginine (arg) and α-(Methylamino)isobutyric acid (meAIB).

Discussion

We report the largest GWAS and the first ExWAS of immunoassay-measured glucagon, GIP and GLP-1, 3 hormones that are central to glucose homeostasis, at both fasting and 120-minutes post-glucose load. This identified 15 hormone-signal associations, including novel associations at *FUT3* for GIP_{T120} and *ABHD15* for GLP-1_{T0}, alongside replication of known loci for GIP (*GIPR*, *ABO* and *SLC5A1*). All 8 glucagon signals were novel, spanning fasting (*ABHD15, PDE3B* and *KLKB1*) and post-glucose measures (*SLC5A1*, *ZNF91, PCSK1, SLC38A4,* and *BCL2*). Secondary analysis of $GIP_{T120-T0}$ highlighted an additional novel gene; *ANO1*. The ExWAS identified 6 novel exome-wide significant associations, highlighting 4 genes: *GCGR* and *PDE3B* for fasting GLP-1 and glucagon; *SAAL1* and *UHMK1* for post-glucose load glucagon and GLP-1 respectively.

These findings highlight the value of studying hormone levels post-glucose load. There were only weak or moderate phenotypic correlations within each hormone between timepoints, and we identified twice as many GWAS signals at T120 than at T0, reflecting the higher heritability estimates at T120 versus T0 across the 3 hormones. This suggests that the hormone response to glucose is under greater genetic control than baseline hormone levels, a finding that should be noted in future studies.

While we convincingly replicated 5 signals, 3 previously reported signals did not replicate in our data. The reason for this is unclear but perhaps relates to differences in the hormone assays: in Almgren *et. al.* GIP was measured by ELISA (EZHGIP-54K, Millipore), total GLP-1 by radioimmunoassay (using either an in-house anti-serum or a commercial kit, GLP1T-36HK), and glucagon by radioimmunoassay (GL-32K)[6]. We used the MSD U-Plex 'sandwich' immunoassay which uses a pair of affinity-optimized monoclonal antibodies combined with MSD electrochemiluminescence (ECL) technology[73]. The use of paired high-affinity antibodies in a sandwich-like design, as in ELISA, is expected to provide higher specificity and a lower standard deviation[74,75]. The ECL further enhances sensitivity and dynamic range beyond standard ELISA[73]. It is possible that cross-reactivity of previous or our current measurements explains the lack of complete replication.

Sandwich immunoassays may also be liable to cross-reactivity between proglucagon-derived peptides. Processing of proglucagon produces several peptides that potentially cross-react with capture antibodies. For GLP-1, a further challenge is to differentiate between intestinal and pancreatic proglucagon products[76]. Glucagon capture antibodies may also recognise alternative proglucagon cleavage products such as oxyntomodulin and glicentin[77]. Alternative proglucagon cleavage peptides which may cross-react with GLP-1 capture antibodies include the major proglucagon fragment and longer inactive forms of GLP-1 (1-37/1-36 amide), which contain the active GLP-1 sequence[78]. We would expect that cross-reactivity would affect glucagon measurements most at T120 when glucagon secretion is low and oxyntomodulin secretion is high. Conversely cross-reactivity would affect GLP-1 measurements most at T0, when L-cell GLP-1 secretion is low, and alpha cells secretion of GLP-1(1-36) is relatively high.

However, our most significant signal for glucagon – at *ZNF91* – did not show a significant association with GLP-1, suggesting that even if there were cross-reactivity, the 2 assays were able to identify distinct genetic architectures.

Despite the success of incretin-based therapies, substantial inter-individual variability in effectiveness and side-effects remains a challenge[79]. Genetic studies can aid this by identifying novel, potentially actionable targets[80]. However, only two of our signals had possible links to BMI; these were the previously established association at *GIPR*, and a robust association at *BCL2*. We found several shared associations with T2D, particularly with GIP_{T120} signals. The observation that two of the strongest associations with GIP at T120 are known regions that related to the human blood group system, suggests a role for blood antigens in the control of the response of GIP to food intake possibly through its stabilisation. Notably, the GWAS signal at *SLC5A1* which encodes the sodium-dependent glucose transporter SGLT1, was the only signal to be associated across all three hormones suggesting a central role in the post-glucose response. The corresponding minor alleles were increasing GIP_{T120}, $GLP\text{-}1_{T120}$, as well as increasing $glucagon_{T120}$, reducing the T2D risk. This may represent a potential treatment target that acts through all 3 hormone pathways.

ANO1 chloride channels, encoded by *ANO1*, contribute to positive regulation of insulin secretion in response to glucose, with previous functional studies suggesting that ANO1 is activated by stimulation of GPCRs[66,67]. Our genetic finding further suggests that GIP secretion may mediate the actions of ANO1 on insulin secretion. This motivated us to undertake GIP secretion assays in human duodenal organoids with WT and *ANO1* knock-out lines. In support of previous work and our hypothesis, stimulating duodenal organoids with agents that elevate cAMP led to significant increase in GIP secretion in the WT line compared to *ANO1* knock-out organoids. This exemplifies the 'genetics-to-mechanism' paradigm, illustrating and supporting the essential role of *ANO1* in regulating GPCR-mediated GIP secretion.

Two of the loci implicate the liver-to-α-cell axis, known to be a key regulator of amino acid metabolism and glucagon secretion. The glucagon receptor (GCGR), highlighted in our exome-based analysis, preferentially couples to *Gs* proteins, stimulating adenylyl cyclase to produce cAMP and triggering signalling cascades[39]. During periods of high systemic glucose demand, glucagon activates this pathway to drive hepatic glycogenolysis and gluconeogenesis[40]. The association of deleterious variants in *GCGR* with higher $glucagon_{T0}$ is consistent with the hyperglucagonemia observed in Mahvash disease, which is characterised by biallelic inactivating *GCGR* mutations, α-cell hyperplasia and early-onset hepatic steatosis, through a breakdown in the liver-to-α-cell axis[81,82]. In glucagon resistance, disruption of normal glucagon-stimulated hepatic amino acid uptake for gluconeogenesis results in downregulation of amino acid transporters such as SLC38A4 in livers, systemic hyperaminoacidemia, compensatory SLC38A4 upregulation in α-cells and glucagon hypersecretion[82,83,88]. A GWAS signal for $glucagon_{T120}$ implicated *SLC38A4* where the $glucagon_{T120}$-increasing allele was associated with increased gene splicing in skeletal muscles and reduced circulating amino acids, mainly alanine. This adds another dimension between glucagon and SLC38A4-mediated amino acid transport in skeletal muscles. Additionally, our in-vitro analysis provides cellular

and islet-based evidence that SLC38A4 modulates α-cell glucagon release. We propose that Na^+-coupled amino acid influx via SLC38A4 induces membrane depolarization and subsequent calcium entry, triggering exocytosis. These findings provide a molecular aetiology for the glucagon kinetics in the liver-to-α-cell axis.
Other loci identified – at *SLC5A1* and *PDE3B* – are also implicated in the associations with branched-chain amino acids levels, supporting the role of amino acids in control of hormone levels.

Based on the *PDE3B* associations highlighted by both GWAS and ExWAS, we suggest there are links between GLP-1 and glucagon with lipid catabolism[27]. Given PDE3B is abundant in adipose tissue and the strong associations that we observe between *PDE3B* and WHR_{adjBMI}, BCAA[31] and ALT levels, we suggest that PDE3B acts as a critical mediator connecting the fasting glucagon signalling to central adiposity and gluconeogenesis.

The novel signal for $glucagon_{T120}$ at *PCSK1* (encoding PC1/3) was not associated with fasting glucagon, or with either GIP or GLP-1 at any timepoint (p>0.05). This is intriguing as it was thought that PC1/3 cleaves intestinal proglucagon and GIP precursor to yield GLP-1 and GIP, respectively; and that glucagon was instead produced by PC2 in pancreatic α-cells. However, recent evidence indicates less tissue-specificity of the convertases on proglucagon than was previously thought[84,85].

In conclusion, by integrating common and rare variant approaches with fasting and post-glucose challenge sampling, we provide novel insights into the genetic regulation of incretins and glucagon. While further experimental validation of the candidate genes is needed, these data provide a resource of potential future therapeutic targets for T2D and obesity. Furthermore, these findings will facilitate genetic causal modelling approaches to predict long-term drug effects. This aligns with the increasingly long-term clinical use of emerging incretin and glucagon targeted therapies, offering a powerful tool to evaluate their potential systemic pleiotropy[86,87].

Material and Methods

Study Description

The Fenland Study (https://studies.epi.ims.cam.ac.uk/fenland) is a population-based cohort of 12,434 participants, born between 1950 and 1975 recruited from general practice surgeries in 3 testing sites: Cambridge, Ely and Wisbech (UK) between 2005 and 2015. Its objective is to explore the role of environmental and genetic factors in determining obesity, type 2 diabetes, and related metabolic disorders. The study and its methods were described in detail previously[88]. Exclusion criteria included pregnancy, prevalent diabetes, an inability to walk unaided, psychosis or terminal illness. The study was approved by the Cambridge Local Research Ethics Committee (NRES Committee – East of England, Cambridge Central, ref. 04/Q0108/19), and all participants provided written informed consent. Biochemical T2D status was defined as either: Glucose at T0 ≥7 mmol/l, Glucose at T120 ≥11.1 mmol/l, or HbA1c ≥48 mmol/mol.

Baseline blood sampling

Using oral glucose tolerance test (OGTT), blood samples for hormone measurements were collected at the baseline study visit in lithium heparin tubes at two timepoints: 1) Fasting (T0), following an overnight fast, and 2) 120 minutes after a drink with 75 grams of oral glucose (T120). Samples were centrifuged at 4°C to separate plasma from blood cells, and plasma stored at −80°C.

Incretin hormone and glucagon measures

In total, 11,342 at T0 and 11,341 at T120 plasma heparin samples were used to measure concentrations of glucagon, total GIP, and total GLP-1. All three analytes were analysed using a multiplex sandwich immunoassay, the Meso Scale Discovery (MSD) U-Plex Custom Metabolic Group 1 assay kit (catalog # K151ACM). Assays were performed according to the manufacturer's protocols (http://www.mesoscale.com/) and as described in *Supp Methods*. Detection ranges were: 3.7-12,500 pg/mL for total GIP, 0.59-576 pM for total GLP-1, and 0.13-156 pM for glucagon. Sample aliquoting was performed using a Hamilton STAR robot, and the measurements were done using MSD Meso Sector S 600 Microplate Reader Imager 1201 with MSD Discovery Workbench® 4.0.13 software.

Trait transformations and definition of change traits

Concentrations of total GIP (pg/mL), total GLP-1 (pM), and glucagon (pM) were inverse rank normal transformed (INT). The change was calculated as the inverse rank normal transformation of the difference between untransformed values at T120 and T0.

Phenotype Correlations

Pearson correlation coefficients were calculated between INT hormone measures, both between the two timepoints for each hormone and between each pair of hormones at the same timepoint. Spearman's correlation was used to assess correlations between raw hormone

concentrations and various metabolic traits, including BMI, HbA1c, insulin at T0 and T120, and Glucose at T0 and T120.

Genotyping and genotype imputation

Genotyping was performed using 3 genotyping arrays: UK Biobank Axiom array, Illumina Infinium HumanCoreExome-24v1, and Affymetrix SNP5.0. Genotyping was performed at Cambridge Genomic Services, Department of Pathology, University of Cambridge, and the Sanger Institute, Cambridge, UK. Standard sample and variant quality control (QC) were performed as described in *Supp Methods*, following which data for 8994 participants were available from Affymetrix Axiom, 1060 from Human CoreExome and 1402 from Affymetrix SNP5.0.

Genotype imputation was performed using the TOPMed reference panel (version r3) for each array individually[89]. Pre-imputation QC was performed as described in *Supp Methods*. Eagle v2[90] was used for haplotype phasing, and the TOPMed Imputation Server for imputation. Then, we combined the three imputed datasets, keeping variants with imputation quality metric r^2 ≥0.3 in at least one array, MAC ≥3 in the combined dataset, and variants with allele frequency differences between any two arrays ≤0.1, leaving 36,320,189 variants for analysis in the combined dataset. Imputation quality (INFO) was calculated for the combined dataset using QCTOOL (v2.2.0) and variants with INFO <0.3 were excluded, leaving 35,706,361variants for downstream analysis. Genomic positions are on genome assembly GRCh38.

Genome-wide association analysis

Genome-wide association analyses were performed using an additive genetic model by BOLT-LMM (version 2.4.1), age, age-squared, sex (self-reported, but consistent with genetic sex), genotyping array and the first ten genetic principal components were included as covariates. Ancestry outliers (defined as those individuals whose principal component score was ≥10 SD from the mean value, for any of the first 10 genetic principal components) were excluded.

GWAS summary statistics QC excluded variants with overall MAF < 0.001, and variants with any of INFO <0.5, or HWE p-value $<1.0\times10^{-7}$ (calculated using qctool_v2.0.2; with -infer-ploidy-from option for variants in non-pseudoautosomal (non-PAR) regions of the X chromosome, which infer sex-specific ploidy from self-reported sex; consequently, deviations from equilibrium are assessed only for the diploid (female) genotypes). Genomic inflation factors (λ) were calculated, and ranged from 1 to 1.047 across the studied traits, indicating adequate control of population stratification and related confounding. Up to 8,559,343 variants remained to be taken forward for further analysis.

The R language and environment for statistical computing (version 4.3.1; R Core Team) was used for analysis, including phenotype transformation, QC of GWAS, and in downstream analysis.

Definition of associated genomic regions and sentinel variants

Distance-based clumping (+/− 250kb) was performed to clump significantly associated genetic variants with $P<5\times10^{-8}$, define associated genomic regions and identify the most significant variants in associated regions as the regional lead variant.

Putative causal gene annotation

We annotated variants using Ensembl Variant Effect Predictor (VEP) v.114[91]. Putative causal genes were assigned using the GWAS-to-gene (G2G) pipeline, which has been described in detail[15]. In brief, G2G calculates gene-level scores based on six sources of genomic and functional evidence, namely: 1) lead variant gene proximity (within +/- 500kb); 2) colocalization with expression quantitative trait locus (eQTL) (using GTEx V7 and eQTLGen data), 3) colocalization with protein QTL (pQTL) data (from UKB-PPP (Pharma Proteomics Project) using Olink[23] and Fenland SomaLogic using SomaScan v4 assay[46]), 4) functional gene prioritization by MAGMA[92] and polygenic priority score (PoPS)[93], 5) overlapping or being in high LD (>80%) with coding variants, 6) overlapping or proximity to an enhancer region using the activity-by-contact (ABC) model. Additionally, we would describe the lead variant as intronic if VEP annotation indicated that the lead variant occurring within an intron. In addition, we looked up whether the lead variant was an eQTL or sQTL using GTEx V10, and the TwinsUK study.

Heritability estimation

We estimated the proportion of phenotypic variation explained by additive genetic effects (narrow-sense heritability) of each trait using Genome-Wide Complex Trait Analysis (GCTA v1.94.1)-Restricted Maximum Likelihood (REML) method, employing a Genetic Relationship Matrix (GRM) generated from common autosomal variants in the combined array-imputed data (excluding ancestry outliers and related individuals)[94]. We excluded variants in the HLA region.We used PLINK (V2.0.) to exclude variants with MAF <0.01, missingness >2%, HWE p-value $<1\times10^{-6}$. Variants were LD-pruned using a 50-variant sliding window with an r^2 threshold of 0.1. Age, age-squared, genotype array, sex, genotyping array and the first ten genetic principal components were adjusted for as covariates.

Proteomics – Olink correlation with Proglucagon

In a subset of 500 randomly selected participants from the Fenland Study, plasma protein levels were measured using the Olink platform, which is based on Olink's proximity extension assay (PEA) technology. Data assessment and quality control measures were performed as described in Pietzner *et al*.[95]. Among the twelve Olink 92-proteins panels, the *Target 96 Cell Regulation Panel* included the prooglucagon protein (Uniprot identifier: P01275), which was quantified in 483 Fenland participants. The Olink assay employed a pair of monoclonal antibodies targeting the first 150 amino acids of proglucagon, enhancing sensitivity and minimising cross-reactivity with alternative proglucagon cleavage products. The reported $\log_{10}$ range was 1.8, with intra-assay variation (mean coefficient of variation, %CV) of 10 and inter-assay %CV of 16, indicating assay performance. For assay validation details, refer to:

https://olink.com/knowledge/documents (see "Validation data - cell regulation" for the relevant file). We assessed correlations between Olink proglucagon measurements and MSD-derived measures of GLP-1 and glucagon in the overlapping subset cohort using Pearson's correlation coefficients.

LD calculations

We conducted linkage disequilibrium (LD) analysis using PLINK (V2.0.) on imputed genotype data from the combined dataset as the reference panel. The analysis is restricted to predefined chromosome regions extending 250kb from the minimum and maximum co-ordinates of significantly associated variants. Only unrelated European individuals were included. The analysis compute pairwise LD estimates (r^2-unphased) between the lead signals and all other variants in the defined region, without applying a minimum LD threshold.

Lookups in common variant GWAS

We performed lookups of common variant associations identified in our GWAS by querying large, well-established and publicly available GWAS summary stats for body mass index (BMI)[69] and waist-hip ratio adjusted for body mass index (WHR_{adjBMI})[96] from up to 700,000 individuals of European genetic ancestry, based on a large GWAS meta-analysis combining the UK Biobank (UKB) and GIANT Consortium cohorts (website: https://giant-consortium.web.broadinstitute.org/index.php/GIANT_consortium_data_files). We queried T2D trans-ancestry GWAS from DIAbetes Genetics Replication And Meta-analysis (DIAGRAM) consortium[97] (website: https://diagram-consortium.org/), composite branched-chain amino acids (sume of the three amino acids: valine, isoleucine, and leucine) GWAS from the European UKB cohort[31]. We queried random glucose[98], fasting glucose (FG), 2hr-glucose post-challenge (2hGlu), glycated haemoglobin (HbA1c), and fasting insulin (FI) GWAS[99] from the Meta-Analysis of Glucose and Insulin-related Traits Consortium (MAGIC) (website: https://www.magicinvestigators.org) (**Supplementary Table 5**). For our GWAS associations of GIP and glucagon, we also queried Olink proteomic GWAS of GIP and proglucagon respectively from the UKB[23] (**Supplementary Table 9**).

First, for each trait, lead signals and proxy variants in pairwise linkage disequilibrium (LD) with the lead signals (r^2-unphased >0.6) were identified within predefined genomic regions. To ensure consistent genomic coordinates across datasets, sentinel and proxy variant positions were harmonized to the GRCh37 reference build. In total, this resulted in 1,978 variants, representing a comprehensive set of candidate loci for downstream lookups. We then examined each GWAS summary stats to determine whether the lead variants or the proxies with the highest LD were reported.

SLC38A4 functional analysis

Expression analysis was performed as described previously[100,101]. Islets were isolated following multiple injections of collagenase V (0.5 mg/ml) into the pancreas of GLU-Venus mice freshly killed by cervical dislocation[101]. Pancreata were digested for 10-11 min at 37°C,

and islets were hand-picked into RPMI. For calcium imaging, islets were dissociated into single cells by trituration in HBSS, plated onto on Matrigel-coated glass coverslips, and cultured overnight in RPMI containing glutamine, fetal calf serum, penicillin and streptomycin. Cells were then loaded with fura2-AM in saline buffer containing 1 mM glucose. α-Cells were identified by their green fluorescence. Ratiometric fura2 imaging (340/380 nm excitation) was performed as described previously (see Reimann *et al.*, methods[101]), in solutions containing 3 mM glucose and additions of different amino acids at 20 mM each. Low sodium experiments were performed by substituting sodium ions with N-methyl-D-gluconate (NMDG) (final [Na+] 5.4 mM). For glucagon secretion studies, whole islets were cultured overnight in RPMI before being divided into Eppendorf tubes (~10 islets per tube), and incubated in saline buffer supplemented with the amino acids indicated for 1 hour at 30°C. Glucagon was measured in cell supernatants by ELISA (MSD), and expressed relative to secretion from parallel tubes of islets incubated without amino acids.

ANO1 functional analysis using GIP secretion assays

Human duodenal organoids maintenance

Human duodenal organoids were derived from anonymised tissue sourced through Addenbrooke's Hospital Tissue Bank (Cambridge, UK) and cultured as previously reported[102,103]. GIP-Venus organoids, which express a yellow fluorescent protein under the control of the GIP promoter, were generated using CRISPR-Cas9 and homology-directed repair (HDR), as previously reported[68]. An *ANO1* knock-out line was generated in these organoids using CRISPR–Cas9-mediated introduction of two targeted double-strand breaks within the gene, leading to disruption through non-homologous end joining (NHEJ). The guides designed for *ANO1* knock-out targeted a 369 bp region, containing an intronic region and exon 11, which encodes transmembrane domain 1 (TMD1) and neighbouring intra- and extracellular loops (GAGAGCACCCCCAACCTGAT**GGG**, TGCACAATTCATTGGGACAC**TGG**). Guide RNAs were cloned into Cas9-expressing plasmids, which were subsequently introduced into cells by electroporation, as described previously[102,103]. Genomic DNA from individually picked clonal organoids were genotyped by PCR amplification, followed by gel electrophoresis analysis of the resulting bands (forward primer: TGGCAGTCGGATAACATCCC; reverse primer: CCTACTGTACAGCCCACGAG). The *ANO1* knock-out positive clones were subsequently expanded, cryopreserved and used in experiments.

GIP secretion assay

Duodenal organoids were cultured for approximately 21 days after passaging, as described previously[68]. Differentiation of GIP-secreting K-cells was confirmed by visualizing Venus positive cells under a fluorescence microscope (EVOS Cell Imaging System). Domes containing organoids were gently detached with ice cold Advanced DMEM/F-12 (Gibco, Thermo Fisher, Bishops Stortford, UK), centrifuged at 400 *g* for 4 minutes, and then digested with 1x TrypLE at 37°C for 6-8 minutes (Gibco, Thermo Fisher, Bishops Stortford, UK). After manual trituration and neutralisation with 10% heat-inactivated FBS, the suspension of single and clustered cells was centrifuged at 400 *g* for 4 minutes and resuspended in organoid culture medium, the composition of which has been described previously[102]. 400 µl of cell suspension

was seeded onto sterile 24-well plates, pre-coated with 4% basement membrane extract, resulting in approximately 80% confluency.

After 18-24 hours, the cells were washed three 3 x 30 minutes with saline buffer (in mmol/l: 138 NaCl, 4.5 KCl, 4.2 $NaHCO_3$, 1.2 NaH_2PO_4, 2.6 $CaCl_2$, 1.2 $MgCl_2$, 10 HEPES; adjusted to pH 7.4 with NaOH) containing 0.01% BSA and 0.1 mM glucose. Following the washes, 200 µl of treatment solution (3-4 repeats per experiment) was added to the wells. After incubation at 37°C for 2 hours, the 200 µl of supernatant was collected, centrifuged at 2000 g for 5 minutes (4°C) and snap-frozen before long-term storage at –80°C. GIP quantification was performed by Core Biochemical Assay Laboratory (CBAL) using the MSD U-plex human GIP (total) assay product (# K1515SK).

Data analysis

Statistical tests were performed in GraphPad Prism (version 11, GraphPad Software, USA). Results were obtained in pg/ml, normalised to the average of 0mM glucose basal treatments and presented as fold changes. Data are means ± SD from 7 independent experiments (3 using GIP-Venus and 4 using *ANO1* knock-out GIP-Venus). D'Agostino-Pearson test was used to assess the normality of the distribution, and unpaired t-test with Welch's correction was applied to test the statistical significance (** indicates $P<0.01$).

Whole-exome sequencing Quality Control

Whole-exome sequencing (WES) was performed at the Wellcome Sanger Institute with variant calling, initial quality control (QC), and functional annotation conducted using the established pipelines as previously described[104,105]. Variant quality was assessed using a random forest-based framework and further benchmarked against UK Biobank data to ensure consistency in variant counts and allele frequencies[106]. Ancestry was assigned by projecting samples onto principal components derived from the 1000 Genomes reference panel[107]. Following QC, 11,512 individuals and ~3.4million high-confidence variants were retained.

Exome-wide burden association testing (ExWAS)

We conducted ExWAS using WES data from individuals of European genetic ancestry as defined in the GWAS methods. ExWAS was performed using an established burden-testing pipeline, using BOLT-LMM v2.4.1[108] under the infinitesimal mixed model with age, age^2, sex, test site, and the first ten PCs as covariates[106]. Variants were annotated using Ensembl VEP v114[91] with REVEL[109], CADD[110], and LOFTEE[111] plugins, with consequences prioritised per gene favouring MANE Select or canonical protein-coding transcripts. We defined Protein Truncating Variants (PTV) as VEP consequence of stop-gained, frameshift, or splice acceptor/donor, while annotations for missense and synonymous variants were adopted directly from VEP.

For burden testing, variants with MAF <1% were aggregated into three partially overlapping functional masks: (1) high-confidence PTV; (2) PTV plus missense variants with a rare exome variant ensemble learner (REVEL) score[109] ≥0.5 (hereafter PTV-REVEL05); and (3) PTV plus

missense variants with a combined annotation-dependent depletion (CADD) score[110] ≥25 (PTV-CADD25). We then filtered gene-mask combinations with a combined carrier count ≥20. To control for multiple testing, a Bonferroni derived exome-wide significance thresholds were derived, correcting for the correlation between masks per trait. This yielded multiple test corrected exome-wide significance thresholds ranging from $P<2.79\times10^{-6}$ (0.05/(11402×1.57)) in GLP-1_{T0} to $P<2.9\times10^{-6}$ (0.05/(11359×1.517)) in GIP_{T0}. Test statistics were well calibrated (λ_{GC} = 1.00-1.04), and no significant associations were observed for masks grouping synonymous variants.

Rare single variant association results

Exome-wide single-variant associations were assessed for variants with a MAC >20. To prioritise rare functional variation, we excluded common variants with MAF >1%, and exome-wide significance was defined as $P<5.0\times10^{-8}$.

Exome-sequence data and quality control in UK Biobank

UK Biobank is a large-scale population prospective study, previously described[112]. Ethics approval for UKB was obtained from the North West Multi-centre Research Ethics Committee (REC reference 13/NW/0157) as a Research Tissue Bank (RTB), with informed consent obtained from all participants. This approval allows researchers to conduct studies without requiring separate ethical clearance, as they are covered by the RTB approval. We performed this research using the UK Biobank Resource under application number 44448.

We accessed whole exome sequence (WES) data on up to 469,835 participants from the UK Biobank (UKB) study (470k WES release, July 2022)[113]. We analysed data on 465,797 individuals after excluding samples with excess heterozygosity, autosomal variant missingness on genotyping arrays ≥5%, or were not included in the subset of phased samples as defined in Bycroft *et al*. [114]. We excluded participants who were not of broadly European genetic ancestry, to perform rare variant burden testing on the European-only UKB samples (n=434,438 individuals). For each outcome, further exclusions were implemented due to incomplete phenotype data (see Supplementary Table 5). Continuous outcome traits were BMI, WHR_{adjBMI}, ALT and HbA1c levels (excluding diabetes cases) while T2D was the only binary outcome. Outcome data were taken from the first UKB study visit, unless otherwise specified in **Supplementary Table 7**.

All data processing and analyses were performed within the UKB Research Analysis Platform (RAP; https://ukbiobank.dnanexus.com/). This is a cloud-based computing environment and the central repository for UKB WES and phenotype data. WES data are stored as population-level variant call format (VCF) files, aligned to GRCh38. In addition to the processing applied to the released data, as documented in Backman *et al.*[113], we performed further quality control measures as described in Gardner *et al.*[115] and detailed in the MRC-EPID WES pipeline (https://github.com/mrcepid-rap/).

Exome-wide burden association testing in UK Biobank

We used BOLT-LMM, a mixed-model algorithm (v2.4.1)[108] to conduct the ExWAS rare-variant burden tests of the significantly associated four genes identified in Fenland ExWAS (*GCGR*, *PDE3B, SAAL1,* and *UHMK1*) toward T2D risk, BMI, WHR_{adjBMI}, ALT and HbA1c. We performed the burden tests of the same three functional masks as defined in the Fenland ExWAS (PTV; PTV-REVEL05; and PTV-CADD25). We used bespoke applets designed for the RAP as described in the MRC-EPID WES pipeline (https://github.com/mrcepid-rap/), including gather code for processing, filtering, annotating and burden testing UKB WES data. All analyses were controlled for sex, age, age^2, the first ten genetic ancestral principal components (PCs) as calculated by Bycroft *et al*. [114], and WES release batch (50k, 200k, 450k).

Tables

Table 1. Baseline characteristics of Fenland study participants with hormone measurements

Trait	Median	25th Centile	75th Centile	N participants
Age (years)	48.8	42.7	54.6	10874
BMI *(*kg/m^2)	26.2	23.6	29.4	10874
Insulin T0 (pmol/l)	40.0	27.0	61.0	10809
Insulin T120 (pmol/l)	185.0	112.0	320.0	10852
Glucose T0 (mmol/l)	4.8	4.5	5.1	10841
Glucose T120 (mmol/l)	5.1	4.2	6.0	10842
HbA1c (mmol/mol)	36.6	34.4	39.0	10832
GIP T0 (pg/mL)	67.8	49.2	94.2	10575
GIP T120 (pg/mL)	378.1	274.1	508.9	10625
GLP-1 T0 (pM)	27.7	22.0	36.0	10648
GLP-1 T120 (pM)	43.1	32.4	59.6	10722
Glucagon T0 (pM)	51.3	37.3	71.3	10679
Glucagon T120 (pM)	37.8	28.4	50.5	10752

*214/12,384 (1.7%) individuals had biochemical T2D status defined as either: Glucose T0 >=7 mmol/l, Glucose T120 >= 11.1 mmol/l, or HbA1c >=48 mmol/mol.

Table 2. Genome-wide-significant signals for GIP, GLP-1 or glucagon at 0 or 120 mins post-oral glucose

Table 2. is attached in an excel file due to the large table size.

Table 3. Rare variant burden test results for GIP, GLP-1 and Glucagon at T0 (fasting) and T120 (120 mins post-oral glucose)

Trait	Gene	MASK	NCAR	NVAR	AC	BETA	SE	*p*
Glucagon T0	*GCGR*	PTV-CADD25	49	18	49	1.068	0.135	2.7E-15
GLP1 T0	*GCGR*	PTV-CADD25	48	17	48	0.756	0.143	1.2E-07
Glucagon T0	*PDE3B*	PTV-REVEL05	102	21	103	-0.605	0.093	9.9E-11
GLP1 T0	*PDE3B*	PTV	30	7	30	-1.097	0.181	1.2E-09
Glucagon T120	*SAAL1*	PTV-REVEL05	21	10	21	-0.964	0.205	2.6E-06
GLP1 T120	*UHMK1*	PTV-CADD25	106	17	106	0.433	0.092	2.7E-06

Trait: All traits underwent inverse normal transformation
MASK: Variant category based on predicted functional impact: (a) PTV: high-confidence protein-truncating variant; (b) PTV-REVEL05: PTV or missense variants with REVEL score >=0.5; and (c) PTV-CADD25: PTV or missense variants with CADD score >= 25
NCAR: number of carriers
NVAR: number of variants
AC: allele count
BETA: effect size estimate
SE: standard error of the effect
p: p value for the association

Data availability

Permission to access the Fenland Study data for analyses through the IMS Epidemiology Trusted Research Environment can be requested by bona fide researchers for specified scientific purposes through an application process via the study website (https://studies.epi.ims.cam.ac.uk/fenland/data-sharing).
The UKB phenotype and WES data used in this study are accessible to registered researchers via the UKB data access protocol. Details on how to register for data access can be found at https://www.ukbiobank.ac.uk/enable-your-research/apply-for-access.

Acknowledgments

The Fenland Study (10.22025/2017.10.101.00001) is funded by the Medical Research Council (MRC) (MC_UU_12015/1). We further acknowledge support for array genotyping from the MRC (MC_PC_13046). Exome Sequencing of the Fenland study was supported by the MRC (MC_PC_23015) and conducted by the Wellcome Trust Sanger Institute. We are grateful to all Fenland volunteers and to the General Practitioners and practice staff for assistance with

recruitment. We thank the Fenland Study Investigators, Fenland Study Co-ordination team and the Epidemiology Field, Data and Laboratory teams.

RD, JM, IDS, JL, NK, KAK, MA, TH, VK, JRBP, KKO and NJW were supported by the Medical Research Council (MC_UU_00006/1, MC_UU_00006/2) and the NIHR Cambridge Biomedical Research Centre (NIHR203312).

For the purpose of Open Access, the author has applied a Creative Commons Attribution (CC BY) licence to any Author Accepted Manuscript version arising.

Contributions

RD, CL, MC, PB, KKO, NJW conceived and designed the project. MA, TH and VK performed the laboratory assays at the IMS Epidemiology laboratories. MA, TH, VK and NDK curated the laboratory results and provided access to the measurements results. RD, JRAM, IDS, JL, KAK curated the genetic data and performed the analyses. SA, AD, GR, RBB, FMG, FR conducted the *SLC38A4* and *ANO1* in vitro experiments and interpreted the laboratory results. RD, JRAM, IDS, FRD, SA, AD, FMG, FR, JRBP, MC, PB, KKO, NJW interpreted the findings and co-wrote the manuscript.

Conflict of Interest Statement

NJW and CL held a research grant with the University of Cambridge from Eli Lilly to support the GLP1, GIP and glucagon measurements in the Fenland study. RD's clinical PhD Fellowship was supported by a grant from Eli Lilly. MC and PB are employees of Eli Lilly.

Figures Legends:

Figure 1. Overview of common and rare variant association analyses for GIP, GLP-1 and glucagon measured at fasting (T0) and 120 minutes post-oral glucose (T120).

Figure 2. Miami plot for GWAS results of GIP measured at fasting (T0) and 120 minutes post-oral glucose (T120). Miami plot showing GIP GWAS results with gene annotation as identified by the GWAS-to-gene (G2G) pipeline. Red dotted lines indicate genome-wide significance threshold at $p = 5\times10^{-08}$. The top panel displays the GWAS of GIP at T120. The bottom panel displays results from the GIP at T0 GWAS.

Figure 3. Miami plot for GWAS results of GLP-1 measured at fasting (T0) and 120 minutes post-oral glucose (T120). Miami plot showing GLP-1 GWAS results with gene annotation as identified by the GWAS-to-gene (G2G) pipeline. Red dotted lines indicate genome-wide significance threshold at $p = 5\times10^{-08}$. The top panel displays the GWAS of GLP-1 at T120. The bottom panel displays results from the GLP-1 at T0 GWAS.

Figure 4. Miami plot for GWAS results of glucagon measured at fasting (T0) and 120 minutes post-oral glucose (T120). Miami plot showing Glucagon GWAS results with gene annotation as identified by the GWAS-to-gene (G2G) pipeline. Red dotted lines indicate genome-wide significance threshold at $p = 5\times10^{-08}$. The top panel displays the GWAS of glucagon at T120. The bottom panel displays results from the glucagon at T0 GWAS.

Figure 5. Functional analysis of *ANO1* using GIP secretion assays. GIP release from WT and ANO1 knock-out human duodenal organoids in response to stimulation with 0mM or 10mM glucose with or without application of Forskolin (10 μM) and IBMX (100μM). Data presented as mean ± SD of the fold change normalised to the average of the 0mM glucose basal treatments. n=8-15 replicates were obtained from 3 to 4 independent experiments. D'Agostino-Pearson test was used to assess the normality of the distribution, and unpaired t-test with Welch's correction was applied to test for statistical significance (** - $P<0.01$).

Figure 6. Functional characterisation of *SLC38A4* expression, amino acid-induced calcium signalling, and glucagon secretion in pancreatic alpha cells. (a) mRNA expression levels in isolated mouse glucagon-producing pancreatic alpha cells, of amino acid transporter group *Slc38a1-5,* determined by RNA sequencing. (b) Validation of amino acid transporter group *Slc38a1-5* expression in isolated mouse alpha cells measured by quantitative PCR (qPCR). (c) Intracellular calcium responses to 20mM of selected amino acids: alanine (ala), glutamine (gln), serine (ser), asparagine (asn), and arginine (arg) recorded in isolated murine alpha cells loaded with the ratiometric calcium indicator dye fura2-AM, with buffer containing 3mM glucose. Each data point represents the peak response of an individual alpha cell (n=1-7 alpha cells per dish, from 4-19 dishes). (d) Paired fura2 fluorescence ratios (340/380 nm) of individual alpha cells stimulated with Serine in standard sodium-containing buffer versus sodium-free buffer where sodium was replaced with *N*-methyl-*D*-glucamine (Serine NMDG). Lines connect responses from the same single cell. (e) Glucagon secretion profiles from

isolated whole intact pancreatic islets in response to the indicated amino acids administered at a concentration of 10mM as following: alanine (ala), glutamine (gln), arginine (arg) and α-(Methylamino)isobutyric acid (meAIB).

References

1. Seino Y, Fukushima M, Yabe D. GIP and GLP-1, the two incretin hormones: Similarities and differences. *J Diabetes Investig* 2010; **1**(1-2): 8-23.
2. Nauck MA, Quast DR, Wefers J, Pfeiffer AFH. The evolving story of incretins (GIP and GLP-1) in metabolic and cardiovascular disease: A pathophysiological update. *Diabetes Obes Metab* 2021; **23 Suppl 3**: 5-29.
3. Baggio LL, Drucker DJ. Biology of incretins: GLP-1 and GIP. *Gastroenterology* 2007; **132**(6): 2131-57.
4. Bergmann NC, Lund A, Gasbjerg LS, et al. Separate and Combined Effects of GIP and GLP-1 Infusions on Bone Metabolism in Overweight Men Without Diabetes. *J Clin Endocrinol Metab* 2019; **104**(7): 2953-60.
5. Helsted MM, Gasbjerg LS, Lanng AR, et al. The role of endogenous GIP and GLP-1 in postprandial bone homeostasis. *Bone* 2020; **140**: 115553.
6. Almgren P, Lindqvist A, Krus U, et al. Genetic determinants of circulating GIP and GLP-1 concentrations. *JCI Insight* 2017; **2**(21).
7. Thareja G, Belkadi A, Arnold M, et al. Differences and commonalities in the genetic architecture of protein quantitative trait loci in European and Arab populations. *Hum Mol Genet* 2023; **32**(6): 907-16.
8. Surapaneni A, Schlosser P, Zhou L, et al. Identification of 969 protein quantitative trait loci in an African American population with kidney disease attributed to hypertension. *Kidney Int* 2022; **102**(5): 1167-77.
9. Suhre K, Arnold M, Bhagwat AM, et al. Connecting genetic risk to disease end points through the human blood plasma proteome. *Nat Commun* 2017; **8**: 14357.
10. Loya H, Kalantzis G, Cooper F, Palamara PF. A scalable variational inference approach for increased mixed-model association power. *Nat Genet* 2025; **57**(2): 461-8.
11. Dhindsa RS, Burren OS, Sun BB, et al. Rare variant associations with plasma protein levels in the UK Biobank. *Nature* 2023; **622**(7982): 339-47.
12. Meeks KAC, Bentley AR, Gouveia MH, et al. Genome-wide analyses of multiple obesity-related cytokines and hormones informs biology of cardiometabolic traits. *Genome Med* 2021; **13**(1): 156.
13. Sun BB, Maranville JC, Peters JE, et al. Genomic atlas of the human plasma proteome. *Nature* 2018; **558**(7708): 73-9.
14. Wareham N. The Fenland Study- investigates the interaction between genetic and lifestyle factors in determining obesity, diabetes and related metabolic disorders which present a considerable public health concern. *http://isrctncom/* 2013.
15. Kentistou KA, Kaisinger LR, Stankovic S, et al. Understanding the genetic complexity of puberty timing across the allele frequency spectrum. *Nat Genet* 2024; **56**(7): 1397-411.
16. Martin MG, Turk E, Lostao MP, Kerner C, Wright EM. Defects in Na+/glucose cotransporter (SGLT1) trafficking and function cause glucose-galactose malabsorption. *Nat Genet* 1996; **12**(2): 216-20.
17. Kamitori K, Shirota M, Fujiwara Y. Structural Basis of the Selective Sugar Transport in Sodium-Glucose Cotransporters. *J Mol Biol* 2022; **434**(5): 167464.
18. Gorboulev V, Schurmann A, Vallon V, et al. Na(+)-D-glucose cotransporter SGLT1 is pivotal for intestinal glucose absorption and glucose-dependent incretin secretion. *Diabetes* 2012; **61**(1): 187-96.

19. Suga T, Kikuchi O, Kobayashi M, et al. SGLT1 in pancreatic alpha cells regulates glucagon secretion in mice, possibly explaining the distinct effects of SGLT2 inhibitors on plasma glucagon levels. *Mol Metab* 2019; **19**: 1-12.
20. Sato Y, Rahman MM, Haneda M, et al. HNF1alpha controls glucagon secretion in pancreatic alpha-cells through modulation of SGLT1. *Biochim Biophys Acta Mol Basis Dis* 2020; **1866**(11): 165898.
21. Knudsen JG, Hamilton A, Ramracheya R, et al. Dysregulation of Glucagon Secretion by Hyperglycemia-Induced Sodium-Dependent Reduction of ATP Production. *Cell Metab* 2019; **29**(2): 430-42 e4.
22. El K, Campbell JE. The role of GIP in alpha-cells and glucagon secretion. *Peptides* 2020; **125**: 170213.
23. Sun BB, Chiou J, Traylor M, et al. Plasma proteomic associations with genetics and health in the UK Biobank. *Nature* 2023; **622**(7982): 329-38.
24. Fatima E, Irfan H, Fatima F, et al. "Is sotagliflozin a 'wonder drug'? A review of its impact on cardiovascular, diabetic, renal, neuroprotective, and hepatic outcomes". *Ann Med Surg (Lond)* 2025; **87**(6): 3700-6.
25. Stockli J, Zadoorian A, Cooke KC, et al. ABHD15 regulates adipose tissue lipolysis and hepatic lipid accumulation. *Mol Metab* 2019; **25**: 83-94.
26. Xia W, Pessentheiner AR, Hofer DC, et al. Loss of ABHD15 Impairs the Anti-lipolytic Action of Insulin by Altering PDE3B Stability and Contributes to Insulin Resistance. *Cell Rep* 2018; **23**(7): 1948-61.
27. DiPilato LM, Ahmad F, Harms M, Seale P, Manganiello V, Birnbaum MJ. The Role of PDE3B Phosphorylation in the Inhibition of Lipolysis by Insulin. *Mol Cell Biol* 2015; **35**(16): 2752-60.
28. Chavez JA, Gridley S, Sano H, Lane WS, Lienhard GE. The 47kDa Akt substrate associates with phosphodiesterase 3B and regulates its level in adipocytes. *Biochem Biophys Res Commun* 2006; **342**(4): 1218-22.
29. Vosa U, Claringbould A, Westra HJ, et al. Large-scale cis- and trans-eQTL analyses identify thousands of genetic loci and polygenic scores that regulate blood gene expression. *Nat Genet* 2021; **53**(9): 1300-10.
30. Koprulu M, Zhao Y, Wheeler E, et al. Identification of Rare Loss-of-Function Genetic Variation Regulating Body Fat Distribution. *J Clin Endocrinol Metab* 2022; **107**(4): 1065-77.
31. Jia RY, Chen JH, Lockhart S, et al. Bidirectional Mendelian Randomization Indicates Causal Relationships Between Circulating Branched-Chain Amino Acids and Metabolic Health. *Diabetes* 2025; **74**(10): 1863-72.
32. Harris BHL, Di Giovannantonio M, Zhang P, et al. New role of fat-free mass in cancer risk linked with genetic predisposition. *Sci Rep* 2024; **14**(1): 7270.
33. Graham SE, Clarke SL, Wu KH, et al. The power of genetic diversity in genome-wide association studies of lipids. *Nature* 2021; **600**(7890): 675-9.
34. Klarin D, Damrauer SM, Cho K, et al. Genetics of blood lipids among ~300,000 multi-ethnic participants of the Million Veteran Program. *Nat Genet* 2018; **50**(11): 1514-23.
35. Sinnott-Armstrong N, Tanigawa Y, Amar D, et al. Genetics of 35 blood and urine biomarkers in the UK Biobank. *Nat Genet* 2021; **53**(2): 185-94.
36. Sakaue S, Kanai M, Tanigawa Y, et al. A cross-population atlas of genetic associations for 220 human phenotypes. *Nat Genet* 2021; **53**(10): 1415-24.

37. Akbari P, Sosina OA, Bovijn J, et al. Multiancestry exome sequencing reveals INHBE mutations associated with favorable fat distribution and protection from diabetes. *Nat Commun* 2022; **13**(1): 4844.
38. Emdin CA, Khera AV, Chaffin M, et al. Analysis of predicted loss-of-function variants in UK Biobank identifies variants protective for disease. *Nat Commun* 2018; **9**(1): 1613.
39. Liu L, Rashid M, Wess J. Regulation of GLP-1 and Glucagon Receptor Function by beta-Arrestins in Metabolically Important Cell Types. *Biochemistry* 2025; **64**(5): 978-86.
40. Rodgers RL. Glucagon, cyclic AMP, and hepatic glucose mobilization: A half-century of uncertainty. *Physiol Rep* 2022; **10**(9): e15263.
41. Bieche I, Manceau V, Curmi PA, et al. Quantitative RT-PCR reveals a ubiquitous but preferentially neural expression of the KIS gene in rat and human. *Brain Res Mol Brain Res* 2003; **114**(1): 55-64.
42. Francone VP, Ifrim MF, Rajagopal C, et al. Signaling from the secretory granule to the nucleus: Uhmk1 and PAM. *Mol Endocrinol* 2010; **24**(8): 1543-58.
43. Mondal N, Dykstra B, Lee J, et al. Distinct human alpha(1,3)-fucosyltransferases drive Lewis-X/sialyl Lewis-X assembly in human cells. *J Biol Chem* 2018; **293**(19): 7300-14.
44. Kukowska-Latallo JF, Larsen RD, Nair RP, Lowe JB. A cloned human cDNA determines expression of a mouse stage-specific embryonic antigen and the Lewis blood group alpha(1,3/1,4)fucosyltransferase. *Genes Dev* 1990; **4**(8): 1288-303.
45. Aubert M, Panicot-Dubois L, Crotte C, et al. Peritoneal colonization by human pancreatic cancer cells is inhibited by antisense FUT3 sequence. *Int J Cancer* 2000; **88**(4): 558-65.
46. Pietzner M, Wheeler E, Carrasco-Zanini J, et al. Mapping the proteo-genomic convergence of human diseases. *Science* 2021; **374**(6569): eabj1541.
47. Cakir B, Heiss G, Pankow JS, et al. Association of the Lewis genotype with cardiovascular risk factors and subclinical carotid atherosclerosis: the Atherosclerosis Risk in Communities (ARIC) study. *J Intern Med* 2004; **255**(1): 40-51.
48. Cheng Y, Li Y, Scherer N, et al. Genetics of osteopontin in patients with chronic kidney disease: The German Chronic Kidney Disease study. *PLoS Genet* 2022; **18**(4): e1010139.
49. Hatanaka T, Huang W, Ling R, et al. Evidence for the transport of neutral as well as cationic amino acids by ATA3, a novel and liver-specific subtype of amino acid transport system A. *Biochim Biophys Acta* 2001; **1510**(1-2): 10-7.
50. Desforges M, Mynett KJ, Jones RL, et al. The SNAT4 isoform of the system A amino acid transporter is functional in human placental microvillous plasma membrane. *J Physiol* 2009; **587**(1): 61-72.
51. Taylor DL, Jackson AU, Narisu N, et al. Integrative analysis of gene expression, DNA methylation, physiological traits, and genetic variation in human skeletal muscle. *Proc Natl Acad Sci U S A* 2019; **116**(22): 10883-8.
52. Kurki MI, Karjalainen J, Palta P, et al. FinnGen provides genetic insights from a well-phenotyped isolated population. *Nature* 2023; **613**(7944): 508-18.
53. Tanaka S, Kurabuchi S, Mochida H, et al. Immunocytochemical localization of prohormone convertases PC1/PC3 and PC2 in rat pancreatic islets. *Arch Histol Cytol* 1996; **59**(3): 261-71.

54. Itoh Y, Tanaka S, Takekoshi S, Itoh J, Osamura RY. Prohormone convertases (PC1/3 and PC2) in rat and human pancreas and islet cell tumors: subcellular immunohistochemical analysis. *Pathol Int* 1996; **46**(10): 726-37.
55. Damholt AB, Buchan AM, Holst JJ, Kofod H. Proglucagon processing profile in canine L cells expressing endogenous prohormone convertase 1/3 and prohormone convertase 2. *Endocrinology* 1999; **140**(10): 4800-8.
56. Martin MG, Lindberg I, Solorzano-Vargas RS, et al. Congenital proprotein convertase 1/3 deficiency causes malabsorptive diarrhea and other endocrinopathies in a pediatric cohort. *Gastroenterology* 2013; **145**(1): 138-48.
57. Meier DT, Rachid L, Wiedemann SJ, et al. Prohormone convertase 1/3 deficiency causes obesity due to impaired proinsulin processing. *Nat Commun* 2022; **13**(1): 4761.
58. Bandsma RH, Sokollik C, Chami R, et al. From diarrhea to obesity in prohormone convertase 1/3 deficiency: age-dependent clinical, pathologic, and enteroendocrine characteristics. *J Clin Gastroenterol* 2013; **47**(10): 834-43.
59. Vogler M, Braun Y, Smith VM, et al. The BCL2 family: from apoptosis mechanisms to new advances in targeted therapy. *Signal Transduct Target Ther* 2025; **10**(1): 91.
60. Saranya Revathy K, Umasuthan N, Whang I, et al. A novel acute phase reactant, serum amyloid A-like 1, from Oplegnathus fasciatus: genomic and molecular characterization and transcriptional expression analysis. *Dev Comp Immunol* 2012; **37**(2): 294-305.
61. Sato T, Fujii R, Konomi K, et al. Overexpression of SPACIA1/SAAL1, a newly identified gene that is involved in synoviocyte proliferation, accelerates the progression of synovitis in mice and humans. *Arthritis Rheum* 2011; **63**(12): 3833-42.
62. Chu PY, Tung SL, Tsai KW, Shen FP, Chan SH. Identification of the Novel Oncogenic Role of SAAL1 and Its Therapeutic Potential in Hepatocellular Carcinoma. *Cancers (Basel)* 2020; **12**(7).
63. Tian Y, Schreiber R, Kunzelmann K. Anoctamins are a family of Ca2+-activated Cl- channels. *J Cell Sci* 2012; **125**(Pt 21): 4991-8.
64. Schreiber R, Uliyakina I, Kongsuphol P, et al. Expression and function of epithelial anoctamins. *J Biol Chem* 2010; **285**(10): 7838-45.
65. Pedemonte N, Galietta LJ. Structure and function of TMEM16 proteins (anoctamins). *Physiol Rev* 2014; **94**(2): 419-59.
66. Yang YD, Cho H, Koo JY, et al. TMEM16A confers receptor-activated calcium-dependent chloride conductance. *Nature* 2008; **455**(7217): 1210-5.
67. Edlund A, Esguerra JL, Wendt A, Flodstrom-Tullberg M, Eliasson L. CFTR and Anoctamin 1 (ANO1) contribute to cAMP amplified exocytosis and insulin secretion in human and murine pancreatic beta-cells. *BMC Med* 2014; **12**: 87.
68. Guccio N, Alcaino C, Miedzybrodzka EL, et al. Molecular mechanisms underlying glucose-dependent insulinotropic polypeptide secretion in human duodenal organoids. *Diabetologia* 2025; **68**(1): 217-30.
69. Yengo L, Sidorenko J, Kemper KE, et al. Meta-analysis of genome-wide association studies for height and body mass index in approximately 700000 individuals of European ancestry. *Hum Mol Genet* 2018; **27**(20): 3641-9.
70. Zhang J, Zheng Y, Martens L, Pfeiffer AFH. The Regulation and Secretion of Glucagon in Response to Nutrient Composition: Unraveling Their Intricate Mechanisms. *Nutrients* 2023; **15**(18).

71. Wada E, Kobayashi M, Kohno D, et al. Disordered branched chain amino acid catabolism in pancreatic islets is associated with postprandial hypersecretion of glucagon in diabetic mice. *J Nutr Biochem* 2021; **97**: 108811.
72. Armour SL, Stanley JE, Cantley J, Dean ED, Knudsen JG. Metabolic regulation of glucagon secretion. *J Endocrinol* 2023; **259**(1).
73. Sloan JH, Siegel RW, Ivanova-Cox YT, Watson DE, Deeg MA, Konrad RJ. A novel high-sensitivity electrochemiluminescence (ECL) sandwich immunoassay for the specific quantitative measurement of plasma glucagon. *Clin Biochem* 2012; **45**(18): 1640-4.
74. Yoshizawa Y, Hosojima M, Kabasawa H, et al. Measurement of Plasma Glucagon Levels Using Mass Spectrometry in Patients with Type 2 Diabetes on Maintenance Hemodialysis. *Kidney Blood Press Res* 2021; **46**(5): 652-6.
75. Brunner M, Moser O, Raml R, et al. Assessment of Two Different Glucagon Assays in Healthy Individuals and Type 1 and Type 2 Diabetes Patients. *Biomolecules* 2022; **12**(3).
76. Deacon CF, Holst JJ. Immunoassays for the incretin hormones GIP and GLP-1. *Best Pract Res Clin Endocrinol Metab* 2009; **23**(4): 425-32.
77. Wewer Albrechtsen NJ, Hartmann B, Veedfald S, et al. Hyperglucagonaemia analysed by glucagon sandwich ELISA: nonspecific interference or truly elevated levels? *Diabetologia* 2014; **57**(9): 1919-26.
78. Bannon CA, Meek CL, Reimann F, Gribble FM. Fasting and post prandial pancreatic and enteroendocrine hormone levels in obese and non-obese participants. *Peptides* 2024; **176**: 171186.
79. Yao H, Zhang A, Li D, et al. Comparative effectiveness of GLP-1 receptor agonists on glycaemic control, body weight, and lipid profile for type 2 diabetes: systematic review and network meta-analysis. *BMJ* 2024; **384**: e076410.
80. Trajanoska K, Bherer C, Taliun D, Zhou S, Richards JB, Mooser V. From target discovery to clinical drug development with human genetics. *Nature* 2023; **620**(7975): 737-45.
81. Cacciottolo TM, Lawler K, Mendez-Acevedo KM, et al. Glucagon Receptor Deficiency Causes Early-Onset Hepatic Steatosis. *Diabetes* 2025; **74**(10): 1787-801.
82. Yu R. Mahvash Disease: 10 Years After Discovery. *Pancreas* 2018; **47**(5): 511-5.
83. Richter MM, Galsgaard KD, Elmelund E, et al. The Liver-alpha-Cell Axis in Health and in Disease. *Diabetes* 2022; **71**(9): 1852-61.
84. Haedersdal S, Andersen A, Knop FK, Vilsboll T. Revisiting the role of glucagon in health, diabetes mellitus and other metabolic diseases. *Nat Rev Endocrinol* 2023; **19**(6): 321-35.
85. Marchetti P, Lupi R, Bugliani M, et al. A local glucagon-like peptide 1 (GLP-1) system in human pancreatic islets. *Diabetologia* 2012; **55**(12): 3262-72.
86. Scott RA, Freitag DF, Li L, et al. A genomic approach to therapeutic target validation identifies a glucose-lowering GLP1R variant protective for coronary heart disease. *Sci Transl Med* 2016; **8**(341): 341ra76.
87. Bowker N, Hansford R, Burgess S, et al. Genetically Predicted Glucose-Dependent Insulinotropic Polypeptide (GIP) Levels and Cardiovascular Disease Risk Are Driven by Distinct Causal Variants in the GIPR Region. *Diabetes* 2021; **70**(11): 2706-19.

88. Lindsay T, Westgate K, Wijndaele K, et al. Descriptive epidemiology of physical activity energy expenditure in UK adults (The Fenland study). *Int J Behav Nutr Phys Act* 2019; **16**(1): 126.
89. Taliun D, Harris DN, Kessler MD, et al. Sequencing of 53,831 diverse genomes from the NHLBI TOPMed Program. *Nature* 2021; **590**(7845): 290-9.
90. Loh PR, Danecek P, Palamara PF, et al. Reference-based phasing using the Haplotype Reference Consortium panel. *Nat Genet* 2016; **48**(11): 1443-8.
91. McLaren W, Gil L, Hunt SE, et al. The Ensembl Variant Effect Predictor. *Genome Biol* 2016; **17**(1): 122.
92. de Leeuw CA, Mooij JM, Heskes T, Posthuma D. MAGMA: generalized gene-set analysis of GWAS data. *PLoS Comput Biol* 2015; **11**(4): e1004219.
93. Weeks EM, Ulirsch JC, Cheng NY, et al. Leveraging polygenic enrichments of gene features to predict genes underlying complex traits and diseases. *Nat Genet* 2023; **55**(8): 1267-76.
94. Yang J, Lee SH, Goddard ME, Visscher PM. GCTA: a tool for genome-wide complex trait analysis. *Am J Hum Genet* 2011; **88**(1): 76-82.
95. Pietzner M, Wheeler E, Carrasco-Zanini J, et al. Synergistic insights into human health from aptamer- and antibody-based proteomic profiling. *Nat Commun* 2021; **12**(1): 6822.
96. Pulit SL, Stoneman C, Morris AP, et al. Meta-analysis of genome-wide association studies for body fat distribution in 694 649 individuals of European ancestry. *Hum Mol Genet* 2019; **28**(1): 166-74.
97. Suzuki K, Hatzikotoulas K, Southam L, et al. Genetic drivers of heterogeneity in type 2 diabetes pathophysiology. *Nature* 2024; **627**(8003): 347-57.
98. Lagou V, Jiang L, Ulrich A, et al. GWAS of random glucose in 476,326 individuals provide insights into diabetes pathophysiology, complications and treatment stratification. *Nat Genet* 2023; **55**(9): 1448-61.
99. Chen J, Spracklen CN, Marenne G, et al. The trans-ancestral genomic architecture of glycemic traits. *Nat Genet* 2021; **53**(6): 840-60.
100. Adriaenssens AE, Svendsen B, Lam BY, et al. Transcriptomic profiling of pancreatic alpha, beta and delta cell populations identifies delta cells as a principal target for ghrelin in mouse islets. *Diabetologia* 2016; **59**(10): 2156-65.
101. Reimann F, Habib AM, Tolhurst G, Parker HE, Rogers GJ, Gribble FM. Glucose sensing in L cells: a primary cell study. *Cell Metab* 2008; **8**(6): 532-9.
102. Goldspink DA, Lu VB, Miedzybrodzka EL, et al. Labeling and Characterization of Human GLP-1-Secreting L-cells in Primary Ileal Organoid Culture. *Cell Rep* 2020; **31**(13): 107833.
103. Miedzybrodzka EL, Foreman RE, Lu VB, et al. Stimulation of motilin secretion by bile, free fatty acids, and acidification in human duodenal organoids. *Mol Metab* 2021; **54**: 101356.
104. Koko M, Fabian L, Popov I, et al. Exome sequencing of UK birth cohorts. *Wellcome Open Res* 2024; **9**: 390.
105. Zakharov G, Eberhardt RY, Frolova A, et al. WxS-QC - a quality control pipeline for human Whole-Genome and Whole Exome sequencing cohorts. *bioRxiv* 2025: 2025.12.15.694327.

106. Perry J, Murzynowski J, Kerrison N, et al. Exploring Rare Genetic Variation Underlying Metabolic Traits in the Fenland Cohort. Springer Science and Business Media LLC; 2026.
107. Genomes Project C, Auton A, Brooks LD, et al. A global reference for human genetic variation. *Nature* 2015; **526**(7571): 68-74.
108. Loh P-R, Tucker G, Bulik-Sullivan BK, et al. Efficient Bayesian mixed-model analysis increases association power in large cohorts. *Nature Genetics* 2015; **47**(3): 284-90.
109. Ioannidis NM, Rothstein JH, Pejaver V, et al. REVEL: An Ensemble Method for Predicting the Pathogenicity of Rare Missense Variants. *Am J Hum Genet* 2016; **99**(4): 877-85.
110. Rentzsch P, Witten D, Cooper GM, Shendure J, Kircher M. CADD: predicting the deleteriousness of variants throughout the human genome. *Nucleic Acids Res* 2019; **47**(D1): D886-D94.
111. Karczewski KJ, Francioli LC, Tiao G, et al. The mutational constraint spectrum quantified from variation in 141,456 humans. *Nature* 2020; **581**(7809): 434-43.
112. Sudlow C, Gallacher J, Allen N, et al. UK biobank: an open access resource for identifying the causes of a wide range of complex diseases of middle and old age. *PLoS Med* 2015; **12**(3): e1001779.
113. Backman JD, Li AH, Marcketta A, et al. Exome sequencing and analysis of 454,787 UK Biobank participants. *Nature* 2021; **599**(7886): 628-34.
114. Bycroft C, Freeman C, Petkova D, et al. The UK Biobank resource with deep phenotyping and genomic data. *Nature* 2018; **562**(7726): 203-9.
115. Gardner EJ, Kentistou KA, Stankovic S, et al. Damaging missense variants in IGF1R implicate a role for IGF-1 resistance in the etiology of type 2 diabetes. *Cell Genom* 2022; **2**(12): None.

R Core Team. *R: A Language and Environment for Statistical Computing* (R Foundation for Statistical Computing, 2023).

Supplementary Files

This is a list of supplementary files associated with this preprint. Click to download.

- Table2GWASsignals.xlsx
- SuppMethod.docx
- Supptables.xlsx